doi:10.1093/plcell/koab137

THE PLANT CELL

THE PLANT CELL 2021: 0: 1–23

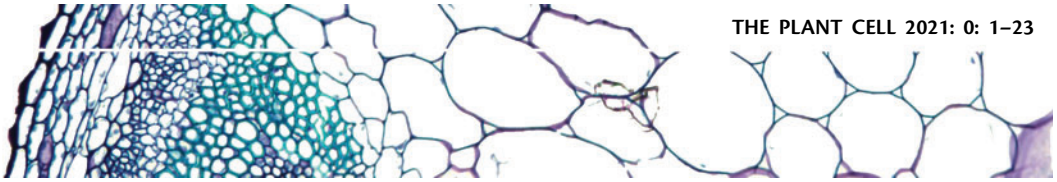

Research Article

WRKY53 integrates classic brassinosteroid signaling and the mitogen-activated protein kinase pathway to regulate rice architecture and seed size

Xiaojie Tian [1], Mingliang He [1,2], Enyang Mei [1,2], Baowen Zhang [3], Jiaqi Tang [1,2], Min Xu [1,2], Jiali Liu [4,5], Xiufeng Li [1], Zhenyu Wang [1], Wenqiang Tang [3], Qingjie Guan [4,5] and Qingyun Bu [1,6,†,*]

1 Key Laboratory of Soybean Molecular Design Breeding, Northeast Institute of Geography and Agroecology, Chinese Academy of Sciences, Harbin 150081, China
2 University of Chinese Academy of Sciences, Beijing 100049, China
3 Ministry of Education Key Laboratory of Molecular and Cellular Biology, Hebei Key Laboratory of Molecular and Cellular Biology, College of Life Sciences, Hebei Normal University, Shijiazhuang 050024, China
4 Key Laboratory of Saline-alkali Vegetation Ecology Restoration (Northeast Forestry University), Ministry of Education, Harbin 150040, China
5 College of Life Science, Northeast Forestry University, Harbin 150040, China
6 The Innovative Academy of Seed Design, Chinese Academy of Sciences, Beijing, China

*Author for correspondence: buqingyun@iga.ac.cn
†Senior author

Q.B. and X.T. conceived and designed the experiments. X.T. performed most of the experiments with the help from M.H., E.M., B.Z., J.T., M.X., J.L., X.L., Z.W., W.T., and Q.G. Q.B. and X.T. analyzed the data and wrote the article.

The author responsible for distribution of materials integral to the findings presented in this article in accordance with the policy described in the Instructions for Authors (https://academic.oup.com/plcell) is: Qingyun Bu (buqingyun@iga.ac.cn).

Abstract

In rice (*Oryza sativa*) and other plants, plant architecture and seed size are closely related to yield. Brassinosteroid (BR) signaling and the mitogen-activated protein kinase (MAPK) pathway (MAPK kinase kinase 10 [MAPKKK10]–MAPK kinase 4 [MAPKK4]–MAPK6) are two major regulatory pathways that control rice architecture and seed size. However, their possible relationship and crosstalk remain elusive. Here, we show that WRKY53 mediated the crosstalk between BR signaling and the MAPK pathway. Biochemical and genetic assays demonstrated that glycogen synthase kinase-2 (GSK2) phosphorylates WRKY53 and lowers its stability, indicating that WRKY53 is a substrate of GSK2 in BR signaling. WRKY53 interacted with BRASSINAZOLE-RESISTANT 1(BZR1); they function synergistically to regulate BR-related developmental processes. We also provide genetic evidence showing that WRKY53 functions in a common pathway with the MAPKKK10–MAPKK4–MAPK6 cascade in leaf angle and seed size control, suggesting that WRKY53 is a direct substrate of this pathway. Moreover, GSK2 phosphorylated MAPKK4 to suppress MAPK6 activity, suggesting that GSK2-mediated BR signaling might also regulated MAPK pathway. Together, our results revealed a critical role for WRKY53 and uncovered sophisticated levels of interplay between BR signaling and the MAPK pathway in regulating rice architecture and seed size.

Received January 10, 2021. Accepted May 06, 2021. Advance access publication May 18, 2021

IN A NUTSHELL

Background: Rice is an important food crop and feeds more than half of the world population. Rice architecture and seed size are closely related to yield. Plant hormone brassinosteroid signaling and the mitogen-activated protein kinase cascade are two major regulatory pathways that control rice architecture and seed size.

Question: To increase the rice yield and breed elite cultivars, it is necessary to identify the critical genes corresponding to architecture and seed size, and utilize them in breeding. Accordingly, we aimed to study the brassinosteroid and mitogen-activated protein kinase signaling pathways in detail, and characterize the major genes involved in the regulation of rice architecture and grain size.

Findings: We found that the transcription factor WRKY53 controls both leaf angle and seed size. GSK2 and BZR1 are two well-known components in rice brassinosteroid signaling. WRKY53 functions downstream of OsGSK2 and in parallel with OsBZR1, and serves as a novel component in brassinosteroid signaling. At the same time, OsWRKY53 is a direct substrate of the mitogen-activated protein kinase pathway. These results suggest that OsWRKY53 might control seed size and leaf angle via mediating the cross-talk between brassinosteroids and the mitogen-activated protein kinase pathway

Next steps: Given that WRKY53 is a transcription factor, we plan to identify the downstream target genes of OsWRKY53, and further investigate the WRKY53-mediated regulatory network involved in rice architecture and seed size control.

Introduction

Brassinosteroids (BRs) are a group of steroid phytohormones that regulate diverse processes such as plant growth, development, and stress responses (Yang et al., 2011). Rice (*Oryza sativa* L.) is an important food crop and feeds more than half of the world population. BRs play important roles in determining rice grain size, tolerance to stress, and plant architecture, including plant height, leaf angle, and tiller number (Zhang et al., 2014). Generally speaking, mutants defective in BR signaling or biosynthesis have erect leaves, dwarf stature, and smaller seeds. Conversely, genotypes with increased BR signaling display wider leaf angles and larger seeds. Therefore, BRs significantly affect the final yield in rice production (Zhang et al., 2014). For example, the rice *dwarf4-1* mutant is defective in BR biosynthesis and has erect leaves, resulting in increased grain yield in high-density planting settings (Sakamoto et al., 2006). Similarly, a slight decrease in the expression of the gene encoding the rice BR receptor BR INSENSITIVE1 (BIN1) leads to erect leaves and higher grain yield, without an accompanying change in grain size (Morinaka et al., 2006). It may thus be feasible to increase rice yield by precisely manipulating BR signaling.

The identification of numerous BR signaling components over the years has allowed the establishment of a working model of the underlying signaling network, providing a global view of BR signaling and molecular mechanisms in *Arabidopsis thaliana* (Kim and Wang, 2010). As the initiating point of the pathway, BRs are recognized by the membrane-localized receptor BRI1 and its co-receptor BRI1-ASSOCIATED RECEPTOR KINASE1 (BAK1), thus forming an active BRI1–BR–BAK1 complex that catalyzes the phosphorylation of cytoplasmic BR SIGNALING KINASEs (BSKs) and CONSTITUTIVE DIFFERENTIAL GROWTH1 (CDG1) (Li and Chory, 1997; Li et al., 2002; Sun et al., 2013). The activating phosphorylation of BSKs and CDG1 leads to the phosphorylation and activation of the protein phosphatase BRI1-SUPPRESSOR 1 (BSU1) (Tang et al., 2008; Kim et al., 2011). One of the BSU1 targets for inactivating dephosphorylation is the Glycogen synthase kinase-3 (GSK3)-like kinase BR-INSENSITIVE 2 (BIN2), which can phosphorylate the transcription factors BRASSINAZOLE (BRZ)-RESISTANT 1 (BZR1) and BRI1 EMS SUPPRESSOR 1 (BES1)(Kim et al., 2009). Finally, nonphosphorylated BZR1 and BES1 translocate to the nucleus and regulate the expression of numerous BR-responsive genes, thus turning on BR signaling (Yin et al., 2005; Sun et al., 2010; Yu et al., 2011). Many Arabidopsis BR signaling components (e.g. BRI1, BAK1, BIN2, BZR1, and BSK) have orthologs in rice and perform conserved functions (Yamamuro et al., 2000; Bai et al., 2007; Li et al., 2009; Tong et al., 2012; Zhang et al., 2016). However, additional signaling components have no clear counterpart in Arabidopsis, including DWARF AND LOW-TILLERING (DLT), TAIHU DWARF1, LEAF AND TILLER ANGLE INCREASED CONTROLLER, BR UPREGULATED 1 (BU1), BU-LIKE 1, INCREASED LAMINA INCLINATION 1, and REDUCED LEAF ANGLE 1 (RLA1; also named SMALL ORGAN SIZE 1, or SMOS1), indicating the possible existence of specific BR signaling branches in rice (Tanaka et al., 2009; Tong et al., 2009; Zhang et al., 2009, 2012; Hu et al., 2013; Hirano et al., 2017; Jang et al., 2017; Qiao et al., 2017). The rice quantitative trait locus *GRAIN LENGTH3* (*qGL3*) encodes a homolog of Arabidopsis BSU1 that negatively regulates BR responses and seed size by dephosphorylating and stabilizing GSK3. Notably, qGL3 displays a function opposite to that of BSU1,

which positively regulates BR signaling, suggesting that orthologous proteins in rice and Arabidopsis may play opposite roles in BR signaling (Gao et al., 2019).

Among classic BR signaling components, BIN2 has a central place in BR signaling as it phosphorylates diverse substrates, each involved in varied developmental processes dependent on BRs (Bai et al., 2007; Tong et al., 2009, 2012; Sun et al., 2015; Yang et al., 2016; Qiao et al., 2017; Xiao et al., 2017; Zhao et al., 2018). Several rice BIN2-like kinases (e.g. GSK1, GSK2, GSK3, and GSK5) have been functionally characterized and shown to share the same negative regulatory role in BR signaling (Koh et al., 2007; Tong et al., 2012; Hu et al., 2018; Gao et al., 2019).

Among these GSK kinases, GSK2 has been extensively studied. The overexpression of mutant forms of *GSK2* and the silencing of *GSK2* by RNA interference (*Gi*) both cause dramatic phenotypic changes in plant height, leaf angle, and seed size (Tong et al., 2012). Many GSK2 substrates have been characterized with diverse functions. For instance, DLT and OVATE family proteins (OFP1 and OFP8) regulate both leaf angle and seed size, while BZR1, CYC U4;1, and RLA1 exclusively control leaf angle (Bai et al., 2007; Tong et al., 2012; Sun et al., 2015; Yang et al., 2016; Qiao et al., 2017; Xiao et al., 2017). Notably, compared to the dramatic phenotypes associated with *GSK2* overexpression (*Go*) and *GSK2* knockdown, the overexpression and mutations of the GSK2 substrates described above show weaker phenotypes (Tong et al., 2012). These results suggest that GSK2 is a core component of BR signaling and that diverse GSK2 substrates might be associated with a subset of GSK2 functions in a tissue- or developmental stage-specific manner. These results also suggest the possibility that GSK2 may have additional, yet-unknown substrates waiting to be identified.

Grain size and shape (i.e. length, width, and thickness) are major factors that affect the yield and quality of rice (Wang et al., 2015; Zhao et al., 2018). Many genes involved in grain size and shape have been identified over the years and have been roughly classified into several pathways: G-protein signaling, the ubiquitin–proteasome pathway, the mitogen-activated protein kinase (MAPK) pathway, BR signaling, transcriptional regulatory factors, and auxin signaling (Li et al., 2019). Each pathway comprises multiple diverse components, with variable degrees of crosstalk between the different pathways, leading to the complexity of the molecular mechanisms determining rice grain size (Li et al., 2019).

A typical MAPK cascade consists of three components: MAPK kinase kinases (MAPKKKs), MAPK kinases (MAPKKs), and MAPKs. MAPK signaling cascades play critical roles in diverse processes such as plant growth, development, and defense against pathogens and predators (Zhang et al., 2018). However, more recent work has also revealed the involvement of MAPK signaling components in the control of rice seed size. For example, the loss of MAPKKK10, MAPKK4, or MAPK6 leads to smaller grains, while their individual constitutive expression results in larger grains (Duan et al., 2014; Liu et al., 2015; Guo et al., 2018; Xu et al., 2018b). Another regulator of this MAPK cascade is MAPK PHOSPHATASE1, which directly interacts with and deactivates MAPK6 to negatively regulate seed size (Guo et al., 2018; Xu et al., 2018a). In addition, the Rho-family GTPase OsRac1 positively regulates cell division and grain size by promoting the phosphorylation and stabilization of MAPK6 (Zhang et al., 2019). Notably, loss of function in either MAPKK4 or MAPK6 resulted in decreased sensitivity to BRs and reduced expression of several BR-related genes, while MAPK PHOSPHATASE 1 (MKP1) mutants displayed the opposite phenotype with hypersensitivity to BRs and elevated expression of BR-related genes (Duan et al., 2014; Liu et al., 2015; Guo et al., 2018). These results suggest that the MAPKKK10—MAPKK4—MAPK6 cascade is involved in crosstalk with BR signaling for the control of seed size in rice. However, the exact details of this relationship and the nature of the crosstalk nodes utilized by the MAPKKK10—MAPKK4–MAPK6 cascade and BR signaling remain elusive, as does the downstream target of the MAPKKK10—MAPKK4—MAPK6 cascade.

We previously demonstrated that the WRKY-type transcription factor WRKY53 positively regulates seed size and various aspects of plant architecture; in addition, the phosphorylation of WRKY53 by the MAPKK4—MAPK6 cascade is indispensable for its biological function, suggesting that WRKY53 might be a target of the MAPKK4—MAPK6 cascade (Tian et al., 2017). We also determined that WRKY53 positively regulates BR signaling and acts genetically downstream of BRI1 (Tian et al., 2017). These results suggest that WRKY53 may participate in both BR signaling and the MAPK pathway. However, how WRKY53 function fits in classic BR signaling is currently unknown.

Here, we show that the loss of WRKY53 function in *Gi* lines largely suppresses the enhanced BR signaling and large seeds seen in *Gi* lines. GSK2 interacts with and phosphorylates WRKY53, leading to the lower stability of the transcription factor, indicating that WRKY53 was a substrate of GSK2. In addition, we show that WRKY53 interacts with BZR1 to synergistically regulate rice BR signaling. Genetic analysis indicated that WRKY53 acts in the same pathway as the MAPKKK10—MAPKK4—MAPK6 cascade to control leaf angle and seed size in rice. Finally, we establish that GSK2 also interacts with and phosphorylates MAPKK4, which lowers MAPK6 activity, indicating that GSK2-meditated BR signaling might also suppress MAPK pathway. Together, these findings reveal the critical role of WRKY53 in BR signaling and illuminate the sophisticated nature of the interplay between BR signaling and the MAPK pathway in rice architecture and seed size control.

Results

WRKY53 genetically acts downstream of GSK2

The fact that the *wrky53* mutant and *WRKY53OE* lines have decreased and increased sensitivity to BRs, respectively, suggested that WRKY53 may positively regulate BR signaling in

rice (Tian et al., 2017). To explore the possible mechanism of this regulation, we investigated the genetic relationship between *WRKY53* and *GSK2*, a critical component of rice BR signaling (Tong et al., 2012). We used a *Gi* line with enhanced BR-related phenotypes to knock out *WRKY53* by genome editing via Clustered Regularly Interspaced Short Palindromic Repeats (CRISPR) and CRISPR-Associated nuclease 9. We then characterized the phenotypes of double mutant *Gi wrky53* line (Supplemental Figure S1). Compared to wild-type (WT) Zhonghua 11 (ZH11), *Gi* displayed much wider leaf angles, but this phenotype was completely suppressed in the *Gi wrky53* background, as this line exhibited leaf angles that were similar to those of ZH11 (Figure 1, A–C; Supplemental Figure S2, A–D). In addition, grains in *Gi wrky53* were markedly shorter than in the *Gi* line (Figure 1, D–F). Moreover, BR-induced lamina inclination assays indicated that the *Gi* line was much more sensitive to BR treatment relative to ZH11, but this increased sensitivity was completely suppressed by the *wrky53* mutation in the *Gi wrky53* background (Figure 1, G and H). The expression levels of BR biosynthesis genes, which are usually the target of a negative feedback regulation by BR signaling, were largely congruent with these results (Bai et al., 2007; Tong et al., 2009; Qiao et al., 2017; Tian et al., 2017). Indeed, the expression of three BR biosynthesis genes (*DWARF2* [*D2*], *DWARF4* [*DWF4*], and *D11*) was markedly lower in the *Gi* line but returned close to WT levels in the *Gi wrky53* background (Figure 1I). Collectively, these results indicated that *Gi wrky53* largely rescues the enhanced BR response seen in the *Gi* line, including leaf angle, seed size, and BR sensitivity.

We also generated a *Gi WRKY53OE* line by crossing the *WRKY53OE* and *Gi* lines. We observed that the *Gi WRKY53OE* line formed wider leaf angles relative to both *WRKY53OE* and *Gi* alone (Supplemental Figure S3, A–E), suggesting additive regulation of leaf angle. In contrast, overexpressing *WRKY53* in the *Gi* background did not further increase grain length or width (Supplemental Figure S3, F–H). Taken together, these results suggest that WRKY53 is indispensable for GSK2 function and acts genetically downstream of GSK2.

WRKY53 and GSK2 play opposite roles

As demonstrated above, WRKY53 acts downstream of GSK2 in rice BR signaling (Figure 1, A–I; Supplemental Figures 2 and 3). To further examine this conclusion and evaluate to what extent WRKY53 affects the GSK2-mediated BR pathway, we harvested flag leaves from wild-type ZH11 and the *Gi* and *Gi wrky53* lines at the heading stage for transcriptome deep sequencing (RNA-seq) and differential gene expression analysis (Figure 1, J–L; Supplemental Figure S4). We identified 5,482 differentially expressed genes between ZH11 and *Gi*, and 3,457 between *Gi* and *Gi wrky53* (Figure 1J; Supplemental Data Set S1). Comparison of these two sets led to the identification of 2,570 overlapping genes that defined a list of genes co-regulated by GSK2 and WRKY53 (Figure 1J; Supplemental Data Set S1). Remarkably, clustering analysis revealed that over 99% of these overlapping genes were oppositely regulated by GSK2 and WRKY53 (Figure 1, K and L; Supplemental Data Set S2). This result strongly supported an opposite role for GSK2 and WRKY53. Gene ontology (GO) analysis of these overlapping genes indicated the involvement of many genes in the BR signaling pathway (Supplemental Figure S4, B and C; Supplemental Data Set S2).

To validate the RNA-seq data, we selected eight genes for RT-qPCR (Reverse Transcription-quantitative realtime Polymerase Chain Reaction) verification. Relative to ZH11, relative transcript levels for *BR-DEFICIENT DWARF1* (*BRD1*), *CYP76M7*, *CYP97C2*, *DWARF4*, and *CYP93G2* were lower in the *Gi* line but almost returned to WT levels in *Gi wrky53*. Likewise, *EARLY RESPONSIVE TO DEHYDRATION1* (*ERD1*), *WRKY72*, and *Cyc1* were more highly expressed in *Gi* but exhibited lower transcript levels closer to those of the WT in *Gi wrky53*, thus verifying our RNA-seq data (Supplemental Figure S5). Taken together, these results suggest that WRKY53 and GSK2 play opposite roles and that WRKY53 acts downstream of GSK2 in regulating downstream gene expression.

WRKY53 interacts with and is phosphorylated by GSK2

GSK2, a GSK3 like kinase and core component of BR signaling, can phosphorylate many substrate proteins (Tong et al., 2012; Che et al., 2015; Sun et al., 2015; Yang et al., 2016; Qiao et al., 2017). The fact that WRKY53 acts downstream of GSK2 prompted us to test whether WRKY53 might be a substrate for GSK2. Bimolecular Fluorescence Complementation (BiFC) and LUC Complementation Imaging (LCI) assays in *Nicotiana benthamiana* leaf epidermal cells indicated that WRKY53 interacts with GSK2 in planta (Figure 2, A and B). Moreover, co-immunoprecipitation (Co-IP) assays confirmed the WRKY53–GSK2 interaction in vivo (Figure 2C; Supplemental Data Set S3).

We then asked whether GSK2 was able to phosphorylate WRKY53. To this end, we performed an in vitro kinase assay with recombinant maltose-binding protein (MBP)-WRKY53 and Glutathione S-Transferase (GST)-GSK2. Indeed, GST-GSK2 phosphorylated both MBP-WRKY53 and itself in vitro (Figure 2D). Importantly, the phosphorylation of MBP-WRKY53 by GST-GSK2 markedly decreased in the presence of increasing amounts of bikinin, a specific inhibitor of BIN2 kinase (Kim et al., 2012), indicating the specificity of this phosphorylation event (Figure 2D).

To extend our results to a plant system, we expressed *MYC-WRKY53* alone or together with *mGSK2-FLAG* in rice protoplasts. In the presence of mGSK2-FLAG, we detected two bands corresponding to MYC-WRKY53, as determined by phos-tag gel analysis (Figure 2E; Supplemental Data Set S3), indicating that GSK2 phosphorylates WRKY53 in vivo. Collectively, these results indicate that GSK2 interacts with and phosphorylates WRKY53. Combined with the

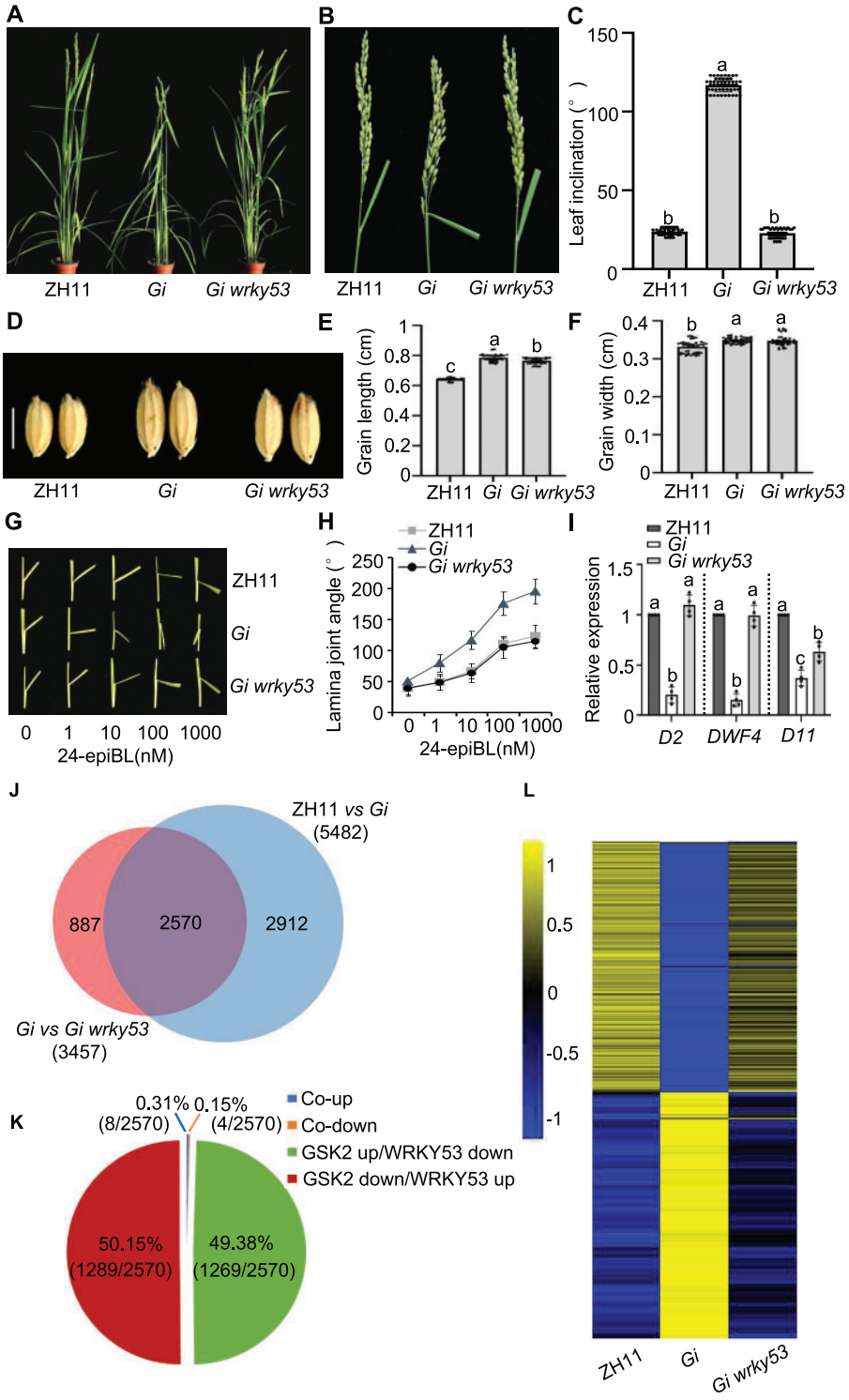

Figure 1 WRKY53 genetically acts downstream of GSK2. A, Gross morphology of ZH11, *Gi*, and *Gi wrky53* at heading stage. B, Lamina joint of flag leaves in ZH11, *Gi*, and *Gi wrky53*. C, Quantification of lamina angles of the flag leaf. Data are means ± SE ($n = 50$). D, Grain phenotype of ZH11, *Gi*, and *Gi wrky53* (scale bar = 5 mm). E and F, Quantification of grain length (E) and grain width (F) in ZH11, *Gi*, and *Gi wrky53*, respectively. Data are means ± SE ($n = 50$). G, Leaf inclination of ZH11, *Gi*, and *Gi wrky53* in the presence of indicated concentration of 24-epiBL. H, Statistical analysis of leaf inclination in (G), Data are means ± SE ($n = 20$). I, RT-qPCR assay showing the relative expression of *D2*, *DWF4*, *D11* in ZH11, *Gi*, and *Gi wrky53*. The expression level in ZH11 was set as "1," data are shown as means ± SE ($n = 4$). J, Venn diagram showing the number of overlapping genes between differentially expressed gene sets of ZH11 versus *Gi*, and *Gi* versus *Gi wrky53*. K, The 2,570 overlapping genes are classified as four classes: GSK2 upregulated and WRKY53 downregulated (green); GSK2 downregulated and WRKY53 upregulated (red); GSK2 and WRKY53 co-upregulated (blue); GSK2 and WRKY53 co-downregulated (orange). The percentage and the number of each class are shown. L, Heatmap showing the expression of 2,570 overlapping genes in ZH11, *Gi*, and *Gi wrky53*. Each dot represents the result from one biological replicate, error bars indicate means ± SE. Statistically significant differences are indicated by different lowercase letters ($P < 0.05$, one-way ANOVA with Tukey's significant difference test).

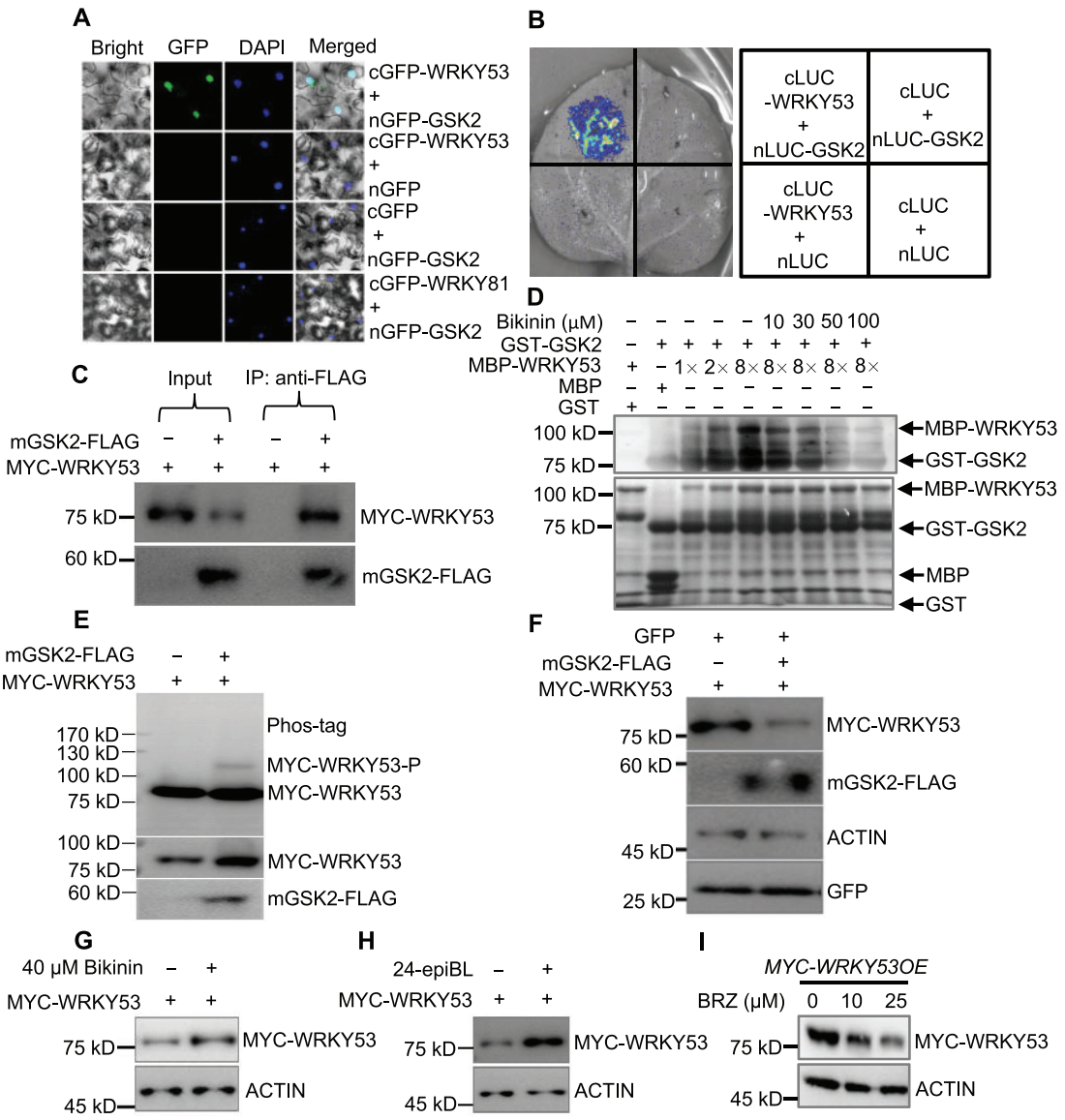

Figure 2 GSK2 phosphorylates and destabilizes WRKY53. A, BiFC assay indicates that WRKY53 interacts with GSK2 in *N. benthamiana* leaves. Co-transformation of cGFP-WRKY53 and nGFP-GSK2 led to the reconstitution of GFP signal, whereas no signal was detected when cGFP-WRKY53 and nGFP, or cGFP and nGFP-GSK2, and cGFP-WRKY81 and nGFP-GSK2 were co-expressed. DAPI (4′,6-diamidino-2-phenylindole) was used to visualize the nuclei. For each interaction pair, at least five independent *N. benthamiana* leaves were infiltrated and analyzed. B, LCI assay indicates that WRKY53 interacts with GSK2 in *N. benthamiana* leaves. Co-transformation of cLUC-WRKY53 and nLUC-GSK2 led to the reconstitution of LUC signal, whereas no signal was detected when cLUC-WRKY53 and nLUC, cLUC and nLUC-GSK2, and cLUC and nLUC were co-expressed. In each experiment, at least five independent *N. benthamiana* leaves were infiltrated and analyzed. C, Co-IP assays indicate that WRKY53 interacts with GSK2 in planta. mGSK2-FLAG and MYC-WRKY53 were co-expressed in rice protoplast. MYC-WRKY53 alone was expressed as control. Protein extract was immunoprecipitated with anti-FLAG antibody and detected with anti-MYC (HRP) (top) or anti-FLAG (HRP) (bottom) antibodies. The un-cropped images and another batch of Co-IP assays lacking the antibody, as a control, are shown in Supplemental Data Set S3. D, In vitro phosphorylation of WRKY53 by GSK2. In vitro phosphorylation reactions were performed using the different combination of purified proteins as indicated. The upper part is the WRKY53 phosphorylation detected by phos-tag Biotin BTL-104. The bottom part is that the equal protein loading in top part was monitored by Coomassie blue staining. E, GSK2 phosphorylates WRKY53 in vivo. mGSK2-FLAG and MYC-WRKY53 were transiently expressed in rice protoplast and cultured for 16 h, MG132 was added at 4 h before collection for protein extraction. The protein was separated on phos-tag gel and common gel and detected by indicated antibody. F, GSK2 destabilizes WRKY53 protein. mGSK2-FLAG, MYC-WRKY53, and GFP were transiently expressed in rice protoplast as indicated, after 16 h incubation, the protein was extracted and used for protein gel blot detected by indicated antibody. G, Bikinin promotes accumulation of WRKY53. MYC-WRKY53 was transiently expressed in rice protoplast, and incubated with and without bikinin for 16 h, and WRKY53 level was examined by protein gel blot with anti-MYC antibody. ACTIN contents detected with anti-ACTIN antibodies were used as loading control. H, BR promotes accumulation of WRKY53. MYC-WRKY53 was transiently expressed in rice protoplast. After 12 h incubation, the protoplast was treated with 24-epiBL for 30 min, and then total protein was extracted and WRKY53 level was examined by protein gel blot with anti-MYC antibody. ACTIN contents detected with anti-ACTIN antibody were used as loading control. I, BRZ destabilizes WRKY53. MYC-WRKY53 plants were grown on MS medium containing indicated concentration of BRZ for 8 days. WRKY53 level was examined by protein gel blot with anti-MYC antibody. ACTIN contents detected with anti-ACTIN antibody were used as loading control. All protein gel blot experiments were repeated at least 3 times with similar results, and the un-cropped images are shown in Supplemental Data Set S3.

fact that WRKY53 acts downstream of GSK2, we propose that WRKY53 is a bona fide GSK2 substrate.

GSK2 decreases WRKY53 stability

Several earlier studies have indicated that GSK2-mediated phosphorylation can lead to destabilization of the substrate protein (He et al., 2002; Chen et al., 2017; Hirano et al., 2017; Qiao et al., 2017; Xiao et al., 2017). To investigate the biochemical relevance of GSK2 phosphorylation on WRKY53, we examined WRKY53 protein levels by transfecting *MYC-WRKY53* alone or together with *mGSK2-FLAG* in rice protoplasts. Co-transfecting *MYC-WRKY53* with *mGSK2-FLAG* significantly decreased the detectable amount of WRKY53, indicating that GSK2 destabilized WRKY53 (Figure 2F; Supplemental Data Set S3). We also examined whether WRKY53 is destabilized by native GSK2. To this end, we transiently expressed *MYC-WRKY53* in rice protoplasts, followed by treatment with the GSK2 inhibitor bikinin. The exogenous application of bikinin promoted the accumulation of MYC-WRKY53 (Figure 2G; Supplemental Data Set S3).

As BRs repress GSK2 activity (He et al., 2002), we next treated protoplasts expressing *MYC-WRKY53* with the 24-epiBL and established that BRs also promoted the accumulation of MYC-WRKY53 (Figure 2H; Supplemental Data Set S3). Last, we grew seedlings overexpressing *MYC-WRKY53* on medium containing the BR biosynthesis inhibitor BRZ and observed a BRZ-dependent decrease in MYC-WRKY53 protein levels (Figure 2I; Supplemental Data Set S3). Collectively, these results indicate that GSK2 negatively affects WRKY53 stability, suggesting that the GSK2-mediated phosphorylation of WRKY53 destabilizes WRKY53 and impairs its biological function, which is in agreement with the finding that GSK2 and WRKY53 play opposite roles.

To determine the biological significance of WRKY53 being phosphorylated by GSK2, we attempted to map the WRKY53 residues phosphorylated by GSK2. We performed an in vitro phosphorylation assay with recombinant WRKY53 and GSK2, followed by mass spectroscopy analysis of phosphorylated WRKY53. We identified seven potential phosphorylation sites in WRKY53: Thr-236, Thr-252, Ser-322, Ser-323, Ser-373, Thr-379, and Thr-401 (Supplemental Figure S6). We then mutated these seven sites to non-phosphorylatable Ala residues, yielding WRKY53(SA), which we used to repeat the in vitro kinase assays. We discovered that the phosphorylation signal of WRKY53(SA) by GSK2 was markedly decreased compared to that of intact WRKY53, indicating that these seven sites are effective sites of WRKY53 phosphorylation by GSK2 (Figure 3A).

To assess the role of these phosphorylation sites in WRKY53 function, we generated lines overexpressing *MYC-WRKY53(SA)* (Supplemental Figure S7, A–G). In parallel, we made the *MYC-WRKY53(SD)* construct, in which all seven phosphorylation sites were mutated from Ser/Thr to Asp to mimic a constitutively phosphorylated form of WRKY53 and generated the corresponding *MYC-WRKY53(SD)* overexpression lines (Supplemental Figure S7, H–N). All *MYC-WRKY53(SA)OE* plants displayed phenotypes similar to *WRKY53OE* lines, including wider leaf angle, larger seeds, and BR hypersensitivity (Figure 3, B–J; Supplemental Figure S7, A–G). Strikingly, all *MYC-WRKY53(SD)OE* lines were phenotypically like the WT, even when expression of the *WRKY53(SD)* transgene reached levels eight-fold higher than the WT (Figure 3, B–J; Supplemental Figure S7, H–N). These results suggested that the phospho-mimic form of WRKY53 might abolish its biological function or be inactive.

Given that GSK2 can phosphorylate WRKY53 and promote its degradation, we assessed the rate of degradation of the WRKY53(SD) and WRKY53(SA) variants by cell-free degradation assays. MYC-WRKY53 was degraded rapidly, but MYC-WRKY53(SA) was degraded slightly more slowly (Figure 3, K and L). In contrast, the degradation rate of MYC-WRKY53(SD) was markedly faster than that of MYC-WRKY53 (Figure 3, K and L). Collectively, these results indicate that the phosphorylation of WRKY53 by GSK2 indeed is biologically relevant and support the notion that GSK2 phosphorylates WRKY53 in vivo.

WRKY53 and BZR1 synergistically regulate rice BR signaling

The above genetic and biochemical data clearly indicated that WRKY53 acts downstream of GSK2 in rice BR signaling (Figures 1–3; Supplemental Figures S2–S7). Many studies have shown that BZR1 is a critical downstream component of BR signaling, and BZR1 has been shown to interact with WRKY46 and its homologs in Arabidopsis to synergistically regulate BR signaling (Wang et al., 2002; Yin et al., 2005; Bai et al., 2007; Sun et al., 2010; Chen et al., 2017). We, therefore, investigated the regulatory relationship between WRKY53 and BZR1 during rice BR signal transduction. To this end, we constructed a *bzr1-D WRKY53OE* line in which both *BZR1* and *WRKY53* are overexpressed (Supplemental Figure S8, A and B; Qiao et al., 2017). Phenotypic analysis showed that from the young seedling to the heading stage, the leaf angle of *bzr1-D WRKY53OE* was significantly wider than with the overexpression of *WRKY53* or *bzr1-D* alone (Figure 4, A–C; Supplemental Figure S8, C and D). Seed size in the *bzr1-D WRKY53OE* line resembled that of *WRKY53OE* (Figure 4, D–F), which is consistent with the observation that *bzr1-D* and *BZR1*-RNAi lines did not exhibit any noticeable change in seed size (Bai et al., 2007; Qiao et al., 2017). A BR sensitivity assay also demonstrated that the *bzr1-D WRKY53OE* line displays a much stronger BR hypersensitivity than either *WRKY53OE* or *bzr1-D* (Figure 4, G and H). These results indicated that WRKY53 and BZR1 synergistically regulate rice BR signaling.

To investigate whether BZR1 and WRKY53 function in parallel, we generated a *bzr1-D wrky53* line by genome editing of *WRKY53* in the *bzr1-D* background (Supplemental Figure S9, A–C). Phenotypic analysis showed that *bzr1-D wrky53* resembles *bzr1-D* for both leaf angle and seed size (Figure 4, I–K; Supplemental Figure S9, D–F). BR-regulated gene expression in *bzr1-D wrky53* was also similar to that

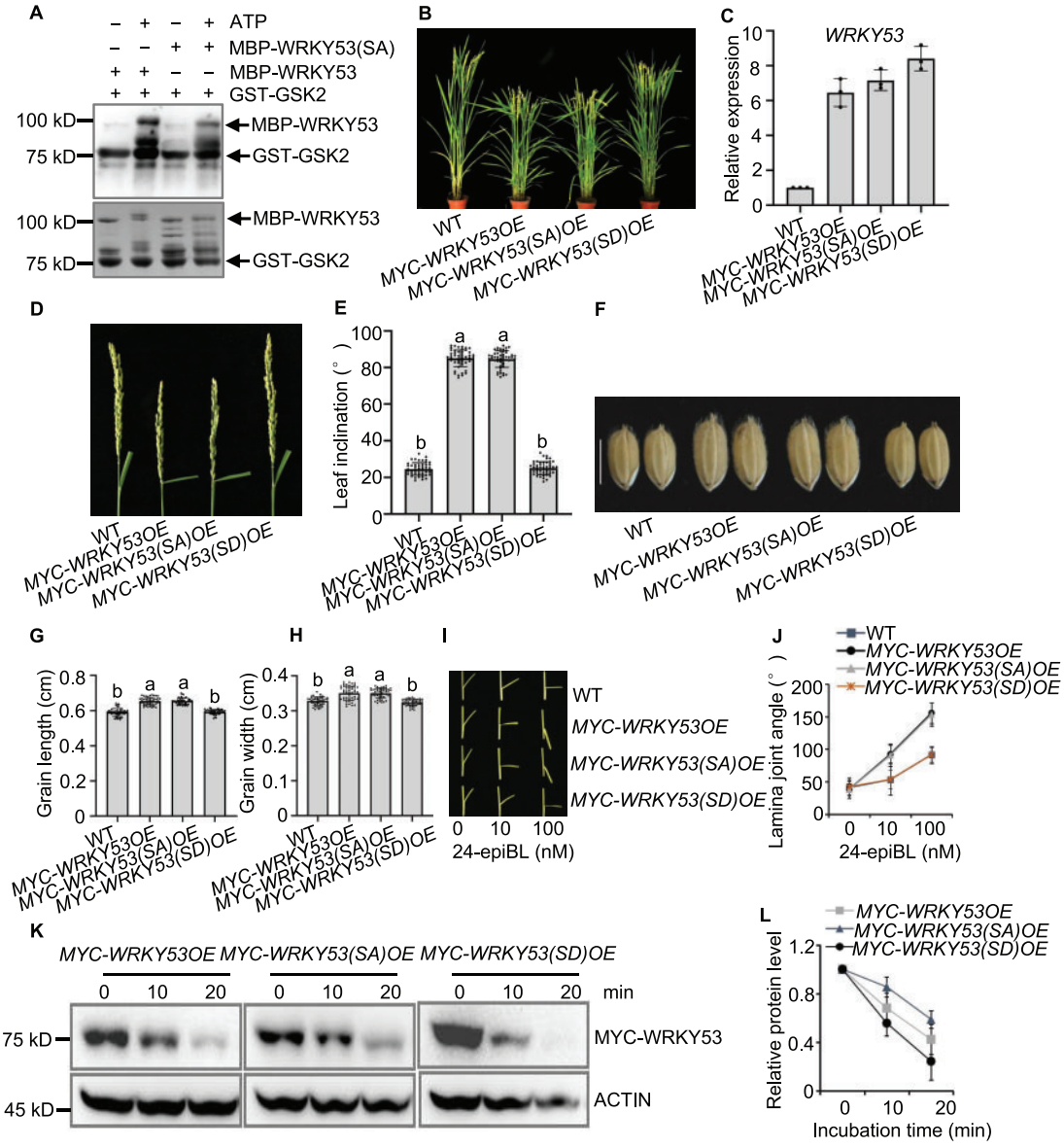

Figure 3 Phosphorylation of WRKY53 by GSK2 abolishes the biological function of WRKY53. A, WRKY53(SA) decreased the phosphorylation of WRKY53 by GSK2. In vitro phosphorylation reactions were performed using the different combination of purified proteins as indicated. The upper part is the WRKY53 phosphorylation detected by Phostag Biotin BTL-104. The bottom part is that the equal protein loading in top part was monitored by Coomassie blue staining. B, The gross morphology of *MYC-WRKY53OE*, *MYC-WRKY53(SA)OE*, and *MYC-WRKY53(SD)OE* at heading stage. C, RT-qPCR assay showing the relative expression of *WRKY53* in representative transgenic plants. The expression level in WT was set as "1," data are shown as means ± SE ($n = 3$). D, Lamina joint of flag leaves in WT, *MYC-WRKY53OE*, *MYC-WRKY53(SA)OE*, and *MYC-WRKY53(SD)OE*. E, Quantification of lamina angles of the flag leaf in (D). Data are means ± SE ($n = 50$). F, Grain phenotype of WT, *MYC-WRKY53OE*, *MYC-WRKY53(SA)OE*, and *MYC-WRKY53(SD)OE* (scale bar = 5 mm). G and H, Quantification of grain length (G) and grain width (H) in WT, *MYC-WRKY53OE*, *MYC-WRKY53(SA)OE*, and *MYC-WRKY53(SD)OE*, respectively. Data are means ± SE ($n = 50$). I, Leaf inclination of WT, *MYC-WRKY53OE*, *MYC-WRKY53(SA)OE*, and *MYC-WRKY53(SD)OE* in the presence of indicated concentration of 24-epiBL. J, Statistical analysis of leaf inclination in (I), Data are means ± SE ($n = 30$). K, Time course of degradation of WRKY53 in *MYC-WRKY53OE*, *MYC-WRKY53(SA)OE*, and *MYC-WRKY53(SD)OE*. Equal amounts of samples were extracted using cell-free degradation buffer, and then incubated for different times before adding the protein loading buffer and boiling. WRKY53 level was examined by protein gel blot with anti-MYC antibody. ACTIN contents detected with anti-ACTIN antibodies were used as loading control. This experiment was repeated five times. L, Quantification of protein degradation speed of WRKY53 in *MYC-WRKY53OE*, *MYC-WRKY53(SA)OE*, and *MYC-WRKY53(SD)OE* in (K). The immunoblot images were quantified by normalizing WRKY53 relative to ACTIN using ImageJ software. The relative protein levels of WRKY53 at 0 min were defined as 1. Data are means ± SE ($n = 5$). The four other biological replications are presented in Supplemental Data Set S3.

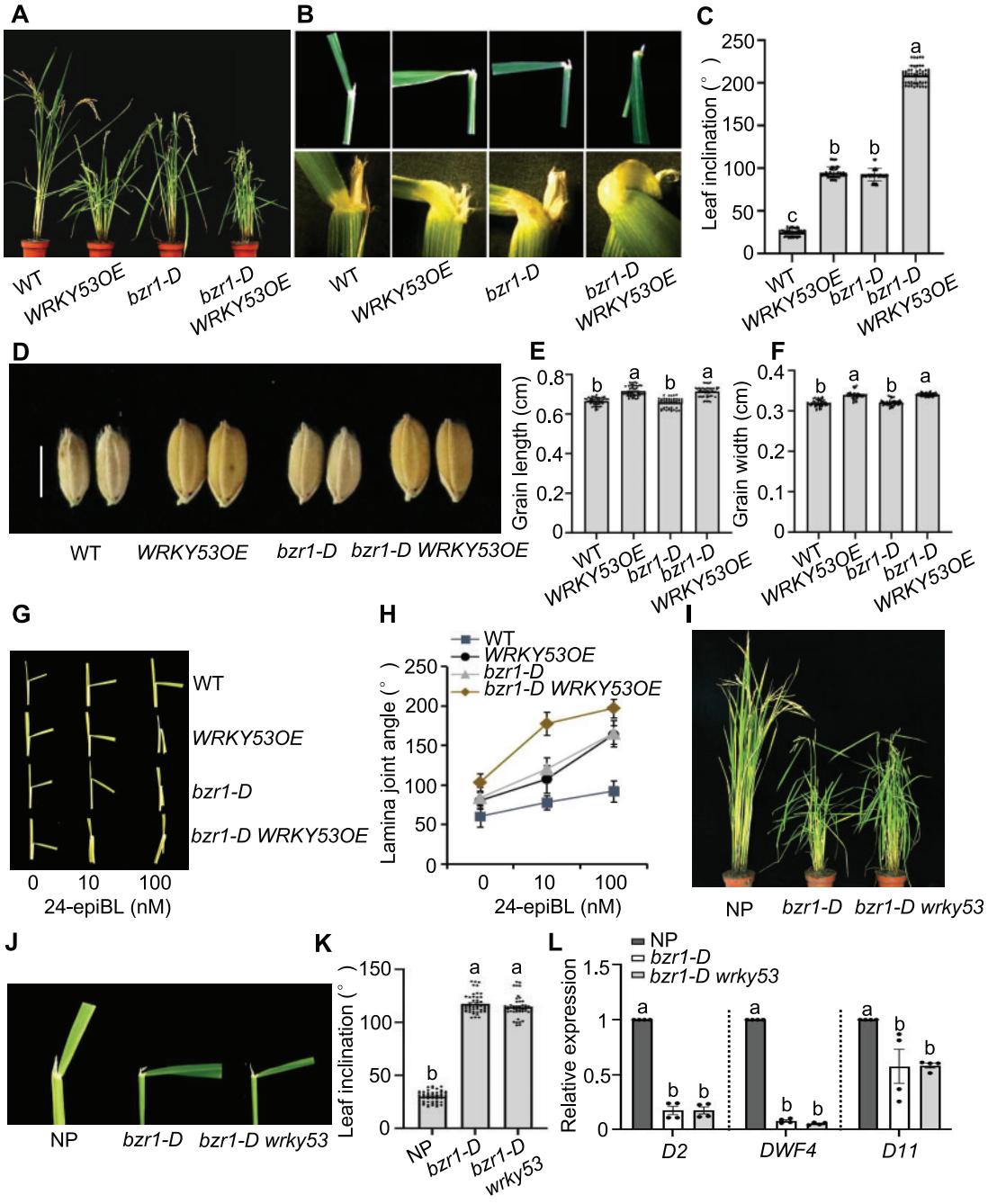

Figure 4 WRKY53 and BZR1 synergistically regulate rice architecture. A, The gross morphology of WT, *WRKY53OE*, *bzr1-D*, *bzr1-D WRKY53OE* at heading stage. B, The lamina joint of flag leaves in WT, *WRKY53OE*, *bzr1-D*, and *bzr1-D WRKY53OE*. The bottom part is magnified leaf node. C, Quantification of lamina angles of the flag leaf (B). Data are means ± SE ($n = 50$). D, The grain phenotype of WT, *WRKY53OE*, *bzr1-D*, *bzr1-D WRKY53OE* (scale bar = 5mm). E and F, Quantification of grain length (E) and grain width (F) in WT, *WRKY53OE*, *bzr1-D*, *bzr1-D WRKY53OE*, respectively. Data are means ± SE ($n = 50$). G, The leaf inclination of WT, *WRKY53OE*, *bzr1-D*, and *bzr1-D WRKY53OE* in the presence of indicated concentration of 24-epiBL. H, Statistical analysis of leaf inclination in (G), Data are means ± SE ($n = 25$). I, Gross morphology of NP, *bzr1-D*, and *bzr1-D wrky53* at heading stage. J, Lamina joint of flag leaves in NP, *bzr1-D*, *bzr1-D wrky53*. K, Quantification of lamina angles of the flag leaf (J). Data are means ± SE ($n = 50$). L, Relative expression of BR-related genes in 2-week-old NP, *bzr1-D*, and *bzr1-D wrky53* plants. Gene expression levels are expressed relative to the value in NP. Error bars indicate means ± SE ($n = 4$). Each dot represents the result from one biological replicate, error bars indicate means ± SE. Statistically significant differences are indicated by different lowercase letters ($P < 0.05$, one-way ANOVA with Tukey's significant difference test).

seen in *bzr1-D* (Figure 4L). Collectively, these results indicate that WRKY53 does not function downstream of BZR1; rather, WRKY53 might function in parallel with BZR1 in the context of BR signaling.

We thus turned to an exploration of a possible biochemical interaction between WRKY53 and BZR1. First, we performed LCI and BiFC assays, which showed that WRKY53 and BZR1 can interact in the nucleus of *N. benthamiana* leaf epidermal cells (Figure 5, A and B). Co-IP assays in rice protoplasts validated their interaction (Figure 5C; Supplemental Data Set S3). These results suggested that WRKY53 and BZR1 might form a complex to co-regulate the expression of common target genes. To test this idea, we selected the *D2* gene as a gene potentially co-regulated by WRKY53 and BZR1, as the *D2* promoter contains both W-box and BRRE cis-elements that are putative binding sites for WRKY53 and BZR1, respectively (Supplemental Figure S10A). Electrophoretic Mobility Shift Assays (EMSAs) demonstrated that indeed, WRKY53 did bind to the W-box in the *D2* promoter (Supplemental Figure S10B). Using the firefly luciferase (LUC) reporter gene driven by the *D2* promoter and WRKY53 and BZR1 as effectors, we observed that BZR1 alone repressed transcription from the *D2* promoter (Figure 5, D–F). Interestingly, *D2* transcription further decreased when WRKY53 and BZR1 were co-expressed (Figure 5F). As specific controls, we mutated the BRRE and W-box elements for transient assay (Figure 5E). Mutating either the BRRE or W-box separately did not markedly affect the synergistic repression of *D2* by BZR1 and WRKY53; however, when the BRRE and W-box elements were both mutated, the synergistic repression of *D2* was largely abrogated and overall repression less pronounced (Figure 5F). These results indicated that WRKY53 and BZR1 act synergistically to regulate BR signaling.

We also used BZR1 as effector and *D2pro-LUC* as a reporter for transient transfection assays in WT rice and the *wrky53* mutant. Transient transfection in the *wrky53* mutant background partially blocked the suppression of *D2* transcription by BZR1 when the amount of BZR1 effector was low, but not with higher amounts, supporting the notion that WRKY53 and BZR1 likely function in parallel (Figure 5G). To further explore whether WRKY53 and BZR1 function synergistically by co-regulating the expression of their common target genes during BR signaling, we re-analyzed the distribution of W-box and BRRE/E-box elements in 2,570 genes co-regulated by WRKY53 and GSK2 in more detail. We determined that the promoters of 81%, 71%, and 70% of WRKY53 and GSK2 co-regulated genes contain a W-box, E-box, or BRRE, respectively (Supplemental Figure S11). Interestingly, both the W-box and BRRE were significantly enriched in the promoters of WRKY53 and GSK2 co-regulated genes, and the W-box was enriched in the promoters of WRKY53 upregulated genes, while the BRRE was enriched in the promoters of WRKY53 downregulated genes (Supplemental Figure S11A). Together, these results suggest that WRKY53 and BZR1 likely function in parallel and synergistically in BR signaling in rice.

WRKY53 functions in a common pathway with MAPK6

MAPK6 was previously shown to phosphorylate WRKY53 (Chujo et al., 2014; Hu et al., 2015; Tian et al., 2017). We also showed that WRKY53 phosphorylation by MAPK6 is indispensable for WRKY53 function, and that MAPK6 promotes WRKY53 activity (Tian et al., 2017). These results indicated that WRKY53 is a putative substrate of MAPK6. To genetically test the hypothesis that WRKY53 acts in a common pathway with MAPK6, we wished to analyze the phenotypes of plants overexpressing one component in a loss-of-function background for the other factor. To this end, we overexpressed *WRKY53* in the *dwarf and small grains 1* (*dsg1*; a weak *mapk6* allele) background (Liu et al., 2015; Supplemental Figure S12, A and B). *dsg1 WRKY53OE* plants formed noticeably wider leaf angle and larger grains than *dsg1* or the wild type (ZH11)(Figure 6, A–E; Supplemental Figure S12A). In parallel, we crossed the *wrky53* mutant with the constitutively active *MAPK6* (*CAMAPK6*) line, which overexpresses a constitutively active form of MAPK6, to generate *CAMAPK6 wrky53* plants (Supplemental Figure S12, C and D). On its own, the *CAMAPK6* line was characterized by larger seeds, as previously reported (Xu et al., 2018b). In contrast, the *CAMAPK6 wrky53* line exhibited a phenotype comparable to that of the *wrky53* single mutant with erect leaf and smaller seed size (Figure 6, F–J; Supplemental Figure S12C), These results indicated that the WRKY53 can suppress the seed size and leaf phenotype caused by MAPK6 function, indicating that WRKY53 acts downstream of MAPK6.

Recently, MKP1 was proposed to negatively regulate seed size by modulating MAPK6 activity (Guo et al., 2018; Xu et al., 2018a). We also generated *MKP1RNAi wrky53* plants by crossing *wrky53* with an *MKP1RNAi* line, in which the expression of *MKP1* transcript levels was significantly reduced by RNA interference (Supplemental Figure S12, E and F). We observed that the *MKP1RNAi* line produced larger seeds, a phenotype similar to *grain size and number 1* (a mutation in *MKP1*) (Guo et al., 2018), but *MKP1RNAi wrky53* displayed a similar phenotype to *wrky53* with smaller seed size and erect leaves, indicating that MKP1 function requires WRKY53 (Figure 6, K–O; Supplemental Figure S12E).

MAPKKK10 was reported to phosphorylate and activate MAPKK4, which then activates MAPK6, and these three kinases appear to function in the same signaling pathway to regulate seed size (Guo et al., 2018; Xu et al., 2018b). We thus overexpressed *WRKY53* in the *small grain2-1* (*smg2-1*; a *mapkkk10* mutant) background (Supplemental Figure S12, G and H). The *smg2-1 WRKY53OE* line had larger grains and formed a wider leaf angle relative to the *smg2-1* single mutant (Figure 6, P–T; Supplemental Figure S12G). Combined with the previous observations that MAPKKK10, MAPKK4, MAPK6, and MKP1 function in a common pathway, and

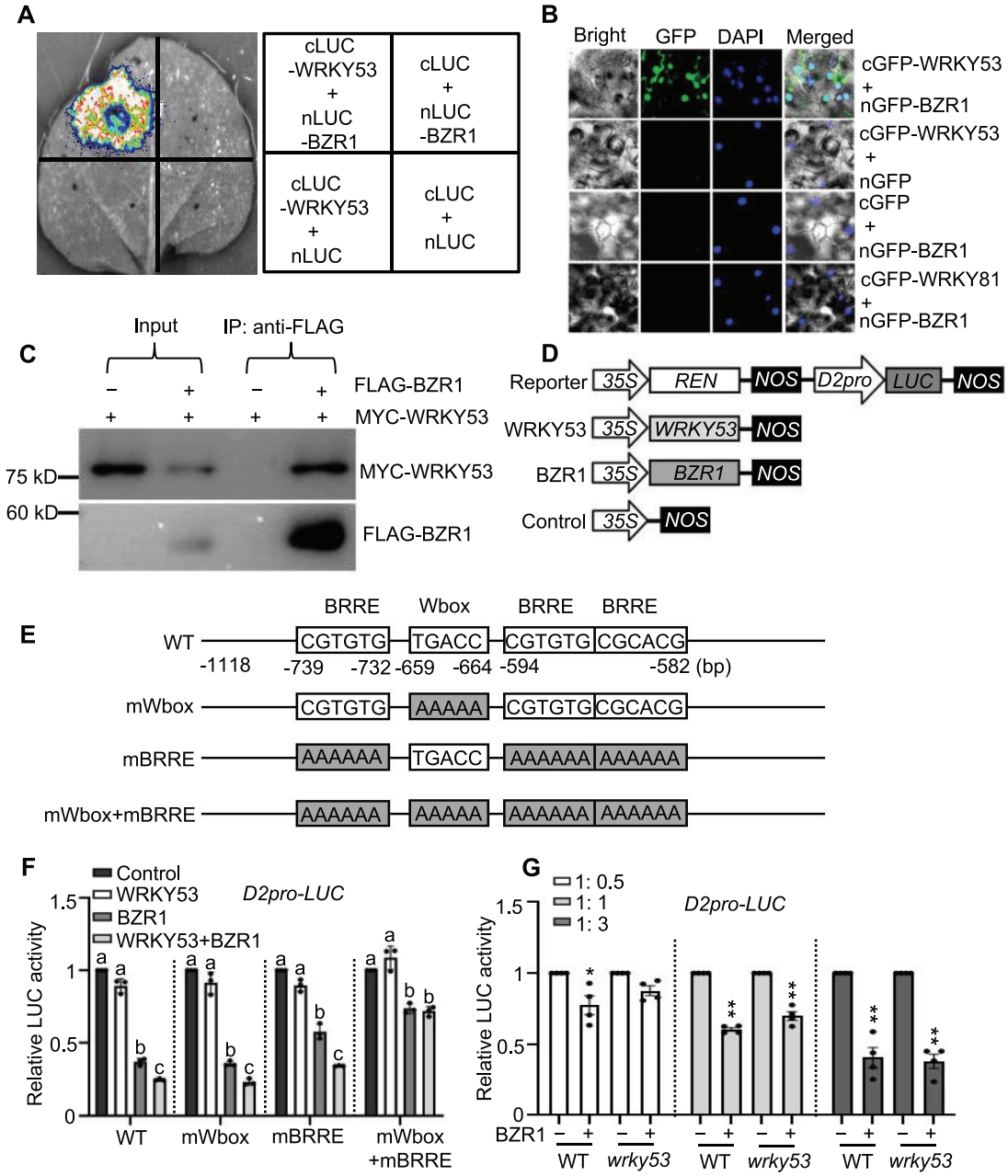

Figure 5 WRKY53 interacts with BZR1 and synergistically regulate rice BR signaling. A, LCI assay indicates that WRKY53 interacts with BZR1 in *N. benthamiana* leaves. Cotransformation of cLUC-WRKY53 and nLUC-BZR1 led to the reconstitution of LUC signal, whereas no signal was detected when cLUC-WRKY53 and nLUC, cLUC, and nLUC-BZR1, and cLUC, and nLUC were co-expressed. In each experiment, at least five independent *N. benthamiana* leaves were infiltrated and analyzed. B, BiFC assay indicates that WRKY53 interacts with BZR1 in *N. benthamiana* leaves. Cotransformation of cGFP-WRKY53 and nGFP-BZR1 led to the reconstitution of GFP signal, whereas no signal was detected when cGFP-WRKY53 and nGFP, or cGFP and nGFP-BZR1, and cGFP-WRKY81 and nGFP-BZR1 were co-expressed. DAPI was used to visualize the nuclei. In each experiment, at least five independent *N. benthamiana* leaves were infiltrated and analyzed. C, Co-IP assay indicates that WRKY53 interacts with BZR1 in planta. FLAG-BZR1 and MYC-WRKY53 were co-expressed in rice protoplasts. MYC-WRKY53 alone was expressed as control. Protein extract was immunoprecipitated with anti-FLAG antibody and detected with anti-MYC (HRP) or anti-FLAG (HRP) antibodies, respectively. Another batch of Co-IP assay using minus antibody as control, and the un-cropped images of independent replications were shown in Supplemental Data Set S3. D, Schematic diagrams of the effector and reporter plasmids used in the transient assay in rice protoplasts. E, Schematic diagram of the promoter region of *D2*. wild-type W-box and BRRE are indicated. mWbox: the mutation of W-box; mBRRE: the mutation of BRRE; mWbox+mBRRE: the mutation of both BRRE and W-box. F, Relative LUC activity in rice protoplasts co-transformed with the indicated reporter and effector plasmids. The LUC activity in control was set as "1." Each dot represents the result from one biological replicate, error bars indicate means ± SE ($n = 3$). Statistically significant differences are indicated by different lowercase letters ($P < 0.05$, one-way ANOVA with Tukey's significant difference test). G, Relative LUC activity in WT and *wrky53* protoplasts co-transformed with indicated the amounts of reporter and effector plasmids. The LUC activity in minus BZR1 was set as "1." Each dot represents the result from one biological replicate, and data are shown as means ± SE ($n = 4$). P-values are comparison between with and without BZR1 and were calculated by Student's *t*-test. *$P < 0.05$, **$P < 0.01$.

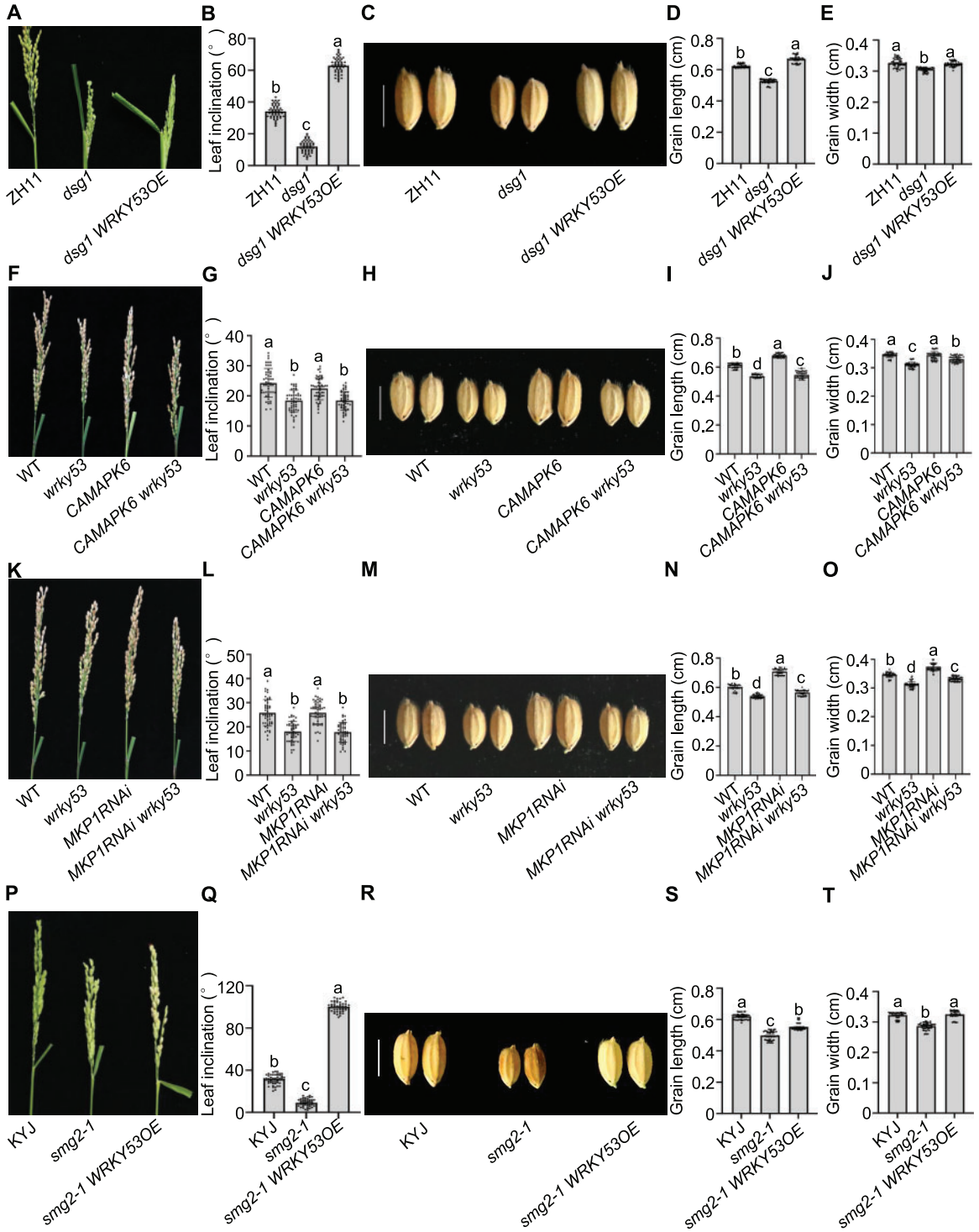

Figure 6 WRKY53 functions in a common pathway with MAPK6. A and B, Phenotype (A) and statistical analysis (B) of flag leaf angle in ZH11, *dsg1*, and *dsg1 WRKY53OE* double mutant plants at heading stage. C–E, Grain morphology (C), quantification of grain length (D), and grain width (E) in ZH11, *dsg1*, and *dsg1 WRKY53OE* double mutant plants. F and G, Phenotype (F) and statistical analysis (G) of flag leaf angle in WT, *wrky53*, *CAMAPK6*, and *CAMAPK6 wrky53* double mutant plants at heading stage. H–J, Grain morphology (H), quantification of grain length (I) and grain width (J) in WT, *wrky53*, *CAMAPK6*, and *CAMAPK6 wrky53* double mutant plants. K and L, Phenotype (K) and statistical analysis (L) of flag leaf angle in WT, *wrky53*, *MKP1RNAi*, and *MKP1RNAi wrky53* double mutant plants at heading stage. M–O, Grain morphology (M), quantification of grain length (N) and grain width (O) in WT, *wrky53*, *MKP1RNAi*, and *MKP1RNAi wrky53* double mutant plant. P and Q, Phenotype (P) and statistical analysis (Q) of flag leaf angle in KYJ, *smg2-1* and *smg2-1 WRKY53OE* double mutant plants at heading stage. R–T, Grain morphology (R), quantification of grain length (S) and grain width (T) in KYJ, *smg2-1*, and *smg2-1 WRKY53OE* double mutant plant. Each dot represents the result from one biological replicate, error bars indicate means ± SE ($n = 50$). Statistically significant differences are indicated by different lowercase letters ($P < 0.05$, one-way ANOVA with Tukey's significant difference test) (scale bar in C, H, K, and P is 5 mm).

that WRKY53 is a substrate for phosphorylation by the MAPKK4–MAPK6 cascade (Tian et al., 2017; Guo et al., 2018; Xu et al., 2018a, 2018b), the above results suggest that WRKY53 is a direct substrate of the MKKK10–MAPKK4–MAPK6 cascade and that WRKY53 functions downstream of this MAPK branch.

Notably, it was reported that GSK2 and the MAPK6 cascade regulate seed size through different mechanisms in which GSK2 mainly regulates cell elongation, while the MAPK6 cascade mainly regulates cell division (Li et al., 2019). To investigate whether WRKY53 controls seed size through modulating cell elongation or cell division, we carried out detailed observations of the outer epidermal cells in lemmas of *WRKY53OE*, *wrky53*, and other related mutants. *WRKY53OE* seeds had increased cell length, and cell number was also moderately increased. In contrast, both cell length and cell numbers were reduced in the *wrky53* mutant (Supplemental Figure S13A), indicating that WRKY53 plays a major role in regulating cell length and minor role in regulating cell proliferation. Similar to WRKY53, examination of *Gi* and *Go* seeds showed that GSK2 also largely regulates cell length and influences cell number to a lesser degree (Supplemental Figure S13B). Interestingly, cell lengths in *Gi wrky53* were markedly shorter than those in the *Gi* line (Supplemental Figure S13C), indicating that WRKY53 functions downstream of GSK2 in seed size. Meanwhile, *dsg1* showed a significantly decreased cell number relative to WT; to our surprise, *CAMAPK6* in two different backgrounds (ZH11 and Longjing 11 [LJ11]) showed significantly increased cell length but similar cell numbers relative to WT (Supplemental Figure S13, D and E). In addition, we examined the *WRKY53SD*^{MAPK6}*OE* and *WRKY53SA*^{MAPK6}*OE* in which the five phosphorylation sites of WRKY53 were mutated to mimic the active or inactive forms of WRKY53 phosphorylated by MAPK6 (Tian et al., 2017). The cell length in *WRKY53SD*^{MAPK6}*OE* was significantly increased compared with *WRKY53OE*, while the cell length in *WRKY53SA*^{MAPK6}*OE* was similar to WT control (Supplemental Figure S13F). These results suggest that MAPK6 and WRKY53 phosphorylated by MAPK6 might be involved in cell expansion. Moreover, cell length of *CAMAPK6 wrky53* was significantly decreased relative to *CAMAPK6* (Supplemental Figure S13G). When we overexpressed *WRKY53* in *dsg1* and *smg2-1* mutants, *WRKY53OE* could greatly increase the cell length, while slightly increasing the cell number in *dsg1* and *smg2-1* mutant backgrounds (Supplemental Figure S13, H and I). These results suggest that WRKY53, at least partially, functions downstream of MAPK6 in regulating seed size. Collectively, we therefore propose that GSK2, MAPK6, and WRKY53 might regulate both cell expansion and cell proliferation to different extents, and thus contribute to the final seed size.

GSK2 phosphorylates MAPKK4 and decreases MAPK6 activity

As described above, GSK2 can phosphorylate and destabilize WRKY53 (Figures 1–3; Supplemental Figures S2–S7). In this and a previous study, we showed that WRKY53 is also phosphorylated by MAPK6 and functions in a common pathway with the MAPKK4–MAPK6 cascade (Tian et al., 2017). Notably, MAPKK4/MAPK6-mediated phosphorylation of WRKY53 may increase WRKY53 DNA-binding activity (Tian et al., 2017). Given that several studies have shown that both GSK2 and the MAPKK4–MAPK6 cascade control rice leaf angle and seed size by regulating BR signaling (Tong et al., 2012; Duan et al., 2014; Liu et al., 2015), we asked whether GSK2 might modulate the MAPKK4–MAPK6 cascade. In Arabidopsis, BIN2 phosphorylates MKK4 and reduces its activity against one of its cognate substrates, MPK6, which itself is part of a signaling module controlling stomatal patterning. BRs thus control stomatal cell fate via BIN2-mediated suppression of MKK4 activity in Arabidopsis (Khan et al., 2013). We, therefore, tested for an interaction between GSK2 and MAPKK4. BiFC and LCI assays showed that GSK2 indeed interacts with MAPKK4 in *N. benthamiana* epidermal cells (Figure 7, A and B). In vitro pull-down assays confirmed this interaction (Figure 7C).

We then examined whether GSK2 phosphorylates MAPKK4. Bioinformatics analysis predicted that MAPKK4 contains 11 putative GSK2 phosphorylation sites (Supplemental Figure S14, A and B). Since MAPKK4 has strong auto-phosphorylation activity, we used a mutant version of the protein, MAPKK4^{K122M} (in which the ATP binding site was mutated) as a substrate for GSK2 phosphorylation (Supplemental Figure S14C). The resulting in vitro kinase assays revealed the stimulation of GST-MAPKK4^{K122M} phosphorylation in the presence of MBP-GSK2, using Phos-tag biotin (Figure 7D). We also noticed the slower migration of GST-MAPKK4^{K122M} by Coomassie blue staining of the SDS–PAGE (Sodium dodecyl sulfate-polyacrylamide gel electrophoresis) gel, indicating that GSK2 indeed phosphorylated MAPKK4 (Figure 7D). In a complementary approach, we transiently expressed *MYC-MAPKK4* construct alone or together with *mGSK2-FLAG* in rice protoplasts. In the presence of mGSK2-FLAG, we detected a slightly stronger signal for the slower migrating band corresponding to phosphorylated MYC-MAPKK4, as detected by phos-tag gel, indicating that GSK2 phosphorylates MAPKK4 in vivo (Figure 7E).

MAPK6 was previously shown to be phosphorylated and activated by MAPKK4 (Yoo et al., 2014; Liu et al., 2015; Tian et al., 2017). We thus asked whether GSK2 might regulate MAPK6 activity by phosphorylating MAPKK4. We performed in vitro kinase assays to test the activity of recombinant GST-MAPKK4DD (a constitutively active form of MAPKK4) against recombinant MBP-MAPK6 as a substrate, with or without added GST-GSK2. We used the anti-pTEpY antibody raised against phospho-p44/42 MAPK to detect phosphorylated MAPK6, as it specifically recognizes the phosphorylated TEY loop motif of MAPKs. In the absence of GST-GSK2, GST-MAPKK4DD phosphorylated MBP-MAPK6, as expected. In contrast, the addition of increasing amounts of GST-GSK2 caused a decrease in phosphorylated MAPK6

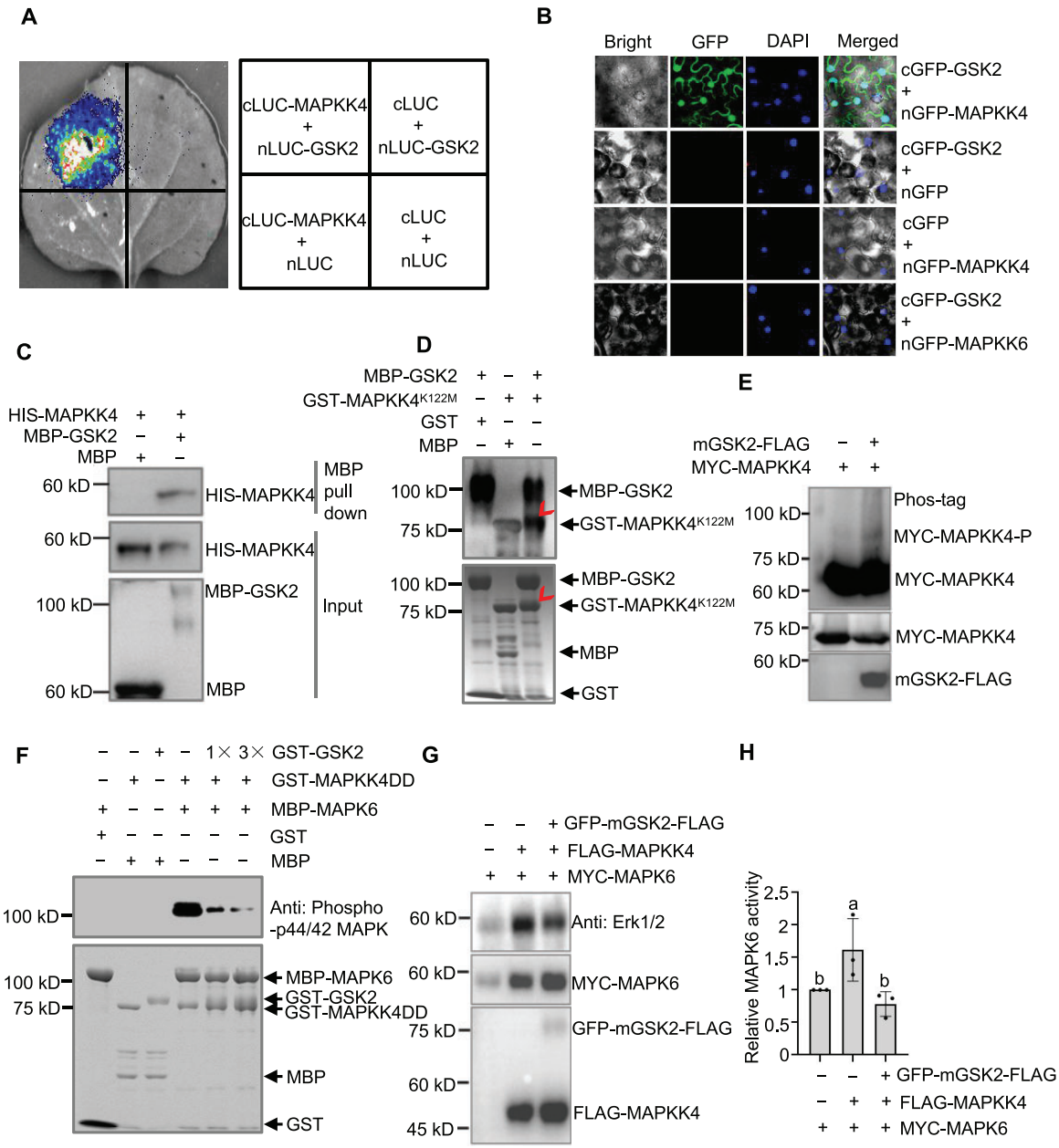

Figure 7 GSK2 phosphorylates MAPKK4 and decrease MAPK6 activity. A, LCI assay indicates that GSK2 interacts with MAPKK4 in *N. benthamiana* leaves. Cotransformation of cLUC-MAPKK4 and nLUC-GSK2 led to the reconstitution of LUC signal, whereas no signal was detected when cLUC-MAPKK4 and nLUC, cLUC and nLUC-GSK2, and cLUC and nLUC were co-expressed. In each experiment, at least five independent *N. benthamiana* leaves were infiltrated and analyzed. B, BiFC assay indicates that GSK2 interacts with MAPKK4 in *N. benthamiana* leaves. Cotransformation of cGFP-GSK2 and nGFP-MAPKK4 led to the reconstitution of GFP signal, whereas no signal was detected when cGFP-GSK2 and nGFP, or cGFP and nGFP-MAPKK4, and cGFP-GSK2 and nGFP-MAPKK6 were co-expressed. DAPI was used to visualize the nuclei. In each experiment, at least five independent *N. benthamiana* leaves were infiltrated and analyzed. C, Pull-down assay showing the interaction between GSK2 interacts with MAPKK4. HIS-MAPKK4 was pulled down by MBP-GSK2 immobilized on amylose resin beads and detected with anti-MBP and anti-HIS antibody, respectively. The un-cropped images of independent replications are shown in Supplemental Data Set S3. D, GSK2 phosphorylates MAPKK4 in vitro. In vitro phosphorylation reactions were performed using the different combination of purified proteins as indicated. The upper part is the MAPKK4 phosphorylation detected by phos-tag Biotin BTL-104. The bottom part is that the equal protein loading in top part was monitored by Coomassie blue staining. Phosphorylated MAPKK4 by GSK2 is indicated by arrow. E, GSK2 phosphorylates MAPKK4 in vivo. mGSK2-FLAG and MYC-MAPKK4 were transiently expressed in rice protoplasts and cultured for 16 h, MG132 was added at 4 h before collection for protein extraction. The protein was separated on phos-tag gel and common gels, and detected by indicated antibody. F, GSK2 decreases MAPK6 activity. The purified MBP-MAPK6, GST-MAPKK4DD, and GST-GSK2 proteins were used for in vitro phosphorylation reactions. The upper part is MAPK6 phosphorylation detected using the anti-phospho-p44/42 MAPK antibody. The bottom part shows equal protein loading monitored by Coomassie blue staining. G, GSK2 decreases MAPK6 activity in vivo. *35S:GFP-mGSK2-FLAG*, *35S:FLAG-MAPKK4*, and *35S:MYC-MAPK6* were transiently expressed in rice protoplast. Phosphorylated MAPK6 was detected using the anti-phospho-p44/42 antibody. The loading

(Figure 7F). We further co-transformed the protoplasts with different combinations of constructs expressing GFP-mGSK2-FLAG, FLAG-MAPKK4, and MYC-MAPK6. We found that MAPKK4 promotes MAPK6 phosphorylation; however, in the presence of GSK2, MAPK6 phosphorylation is significantly decreased (Figure 7, G and H; Supplemental Data Set S3), indicating that GSK2 decreases MAPK6 phosphorylation in vivo. Taken together, these results suggest that GSK2 negatively regulates MAPK6 activity through the inactivating phosphorylation of MAPKK4.

Genetic relationship between MAPKK4−MAPK6 and GSK2

Mutants with loss of function in either MAPKK4 or MAPK6 have decreased BR sensitivity, erect leaf, and smaller seeds, while *Gi* lines have enhanced BR sensitivity, increased leaf angle, and larger seeds (Tong et al., 2012; Duan et al., 2014; Liu et al., 2015). In this study, we found that GSK2 negatively regulates MAPK6 activity by phosphorylating the upstream kinase MAPKK4 (Figure 7), suggesting that MAPKK4–MAPK6 might participate in GSK2-mediated biological function. To test this possibility, we crossed the *Gi* line with *smg1-1* (a *mapkk4* mutant) to generate the *Gi smg1-1* line (Figure 8A; Supplemental Figure S15A). The *Gi* line and the *smg1-1* mutant exhibit opposite effects on both seed size and leaf angle (Tong et al., 2012; Duan et al., 2014). Interestingly, seeds from the *Gi smg1-1* line were phenotypically similar to the *smg1-1* single mutant, while the leaf angle of *Gi smg1-1* line was like that of *Gi* (Figure 8, A–F). We also generated a *Gi dsg1* line by crossing the *Gi* line with the weak *mapk6* mutant allele *dsg1* (Figure 8G; Supplemental Figure S16A). Again, the *Gi dsg1* line showed similar seed size to *dsg1*, but similar leaf angle to *Gi* (Figure 8, G–L). Cell analysis showed that, compared with *Gi*, the cell number of *Gi dsg1* and *Gi smg1-1* was greatly decreased, while cell length of *Gi dsg1* and *Gi smg1-1* was slightly decreased (Supplemental Figures S15B and S16B). These results suggest that GSK2 might function in parallel with MAPKK4–MAPK6. Nevertheless, we cannot rule out the possibility that GSK2 functions upstream of MAPK in some specific process; since GSK2 has multiple substrates to control diverse processes (Tong and Chu, 2018), mutation of a single MAPK signaling component is not enough to reverse the entirety of GSK2 function.

Discussion

WRKY53 is a crucial downstream component of GSK2 for BR signaling

Many BR signaling components have been characterized and their underlying mechanisms deciphered in rice (Zhang et al., 2014; Sun et al., 2015; Qiao et al., 2017). Although we previously showed that WRKY53 can positively regulate BR responses in rice, how WRKY53 contributes BR signaling was not clear (Tian et al., 2017). In this study, we provide substantial evidence to support the hypothesis that WRKY53 is a crucial component of BR signaling. The *Gi wrky53* line largely suppressed the phenotypes associated with silencing of *GSK2* in the *Gi* line, including seed size, leaf angle, BR-regulated gene expression, and BR sensitivity (Figure 1, A–I; Supplemental Figure S2). Likewise, the *Gi WRKY53OE* line showed additive phenotypes above those of *WRKY53OE* and *Gi* alone for leaf inclination (Supplemental Figure S3). Transcriptome analysis indicated that WRKY53 and GSK2 play opposite roles in the regulation of downstream gene expression (Figure 1, J–L; Supplemental Figures S4 and S5). More importantly, we established that WRKY53 restored the expression of ∼46.9% of GSK2-regulated genes relative to the *Gi* line (Figure 1J). These results indicate that WRKY53 plays a crucial role in BR signaling and acts genetically downstream of GSK2. In addition, GSK2 interacts with and phosphorylates WRKY53 (Figure 2, A–E). We mapped seven major GSK2 phosphorylation sites on WRKY53, and a phospho-mimic version of WRKY53 abolished its biological function (Figure 3; Supplemental Figures S6 and S7). Unfortunately, given that WRKY53 is a very unstable protein for unknown reasons, we failed to directly observe the phosphorylated form of WRKY53 in WT and *Gi*. It remains to be further investigated exactly when and where this phosphorylation occurs in plants. Combined with our genetic analysis (Figure 1, A–I; Supplemental Figures S2 and S3), we propose that WRKY53 is a substrate of GSK2 (Figure 9). WRKY53, like the other GSK2 substrates DLT, OFP1, and OFP8, regulates both leaf angle and seed size, in contrast to BZR1, CYC U4;1, and RLA, which exclusively regulate leaf angle (Bai et al., 2007; Tong et al., 2012; Sun et al., 2015; Yang et al., 2016; Qiao et al., 2017; Tian et al., 2017). These results indicate that GSK2 has diverse substrates and can regulate multiple developmental processes through their regulated phosphorylation. Recently, OsGSK3 and OsGSK5 were also shown to act in BR signaling and control of seed size (Hu et al., 2018; Gao et al., 2019). It will be interesting to determine if OsGSK3 and OsGSK5 might share substrates with GSK2, and whether WRKY53 performs similar functions in OsGSK3- and OsGSK5-mediated signaling.

WRKY53 functions synergistically with BZR1 in BR signaling

Based on this study, we propose that WRKY53 functions in parallel with BZR1, but not downstream of BZR1. The evidence supporting this claim is as follows. First, the leaf angle phenotype and BR sensitivity seen in the *bzr1-D WRKY53OE*

control of MAPKK4, GSK2, and MAPK6 was detected using the anti-MYC and anti-FLAG antibody, respectively. H, Quantification of relative MAPK6 activity of (G). The immunoblot images were quantified by normalizing phosphorylated MAPK6 relative to MYC-MAPK6 using ImageJ software. The relative MAPK6 activity of the protoplasts with MYC-MAPK6 alone was defined as 1. Data are means ± SE ($n = 3$). The two other biological replications are presented in Supplemental Data Set S3.

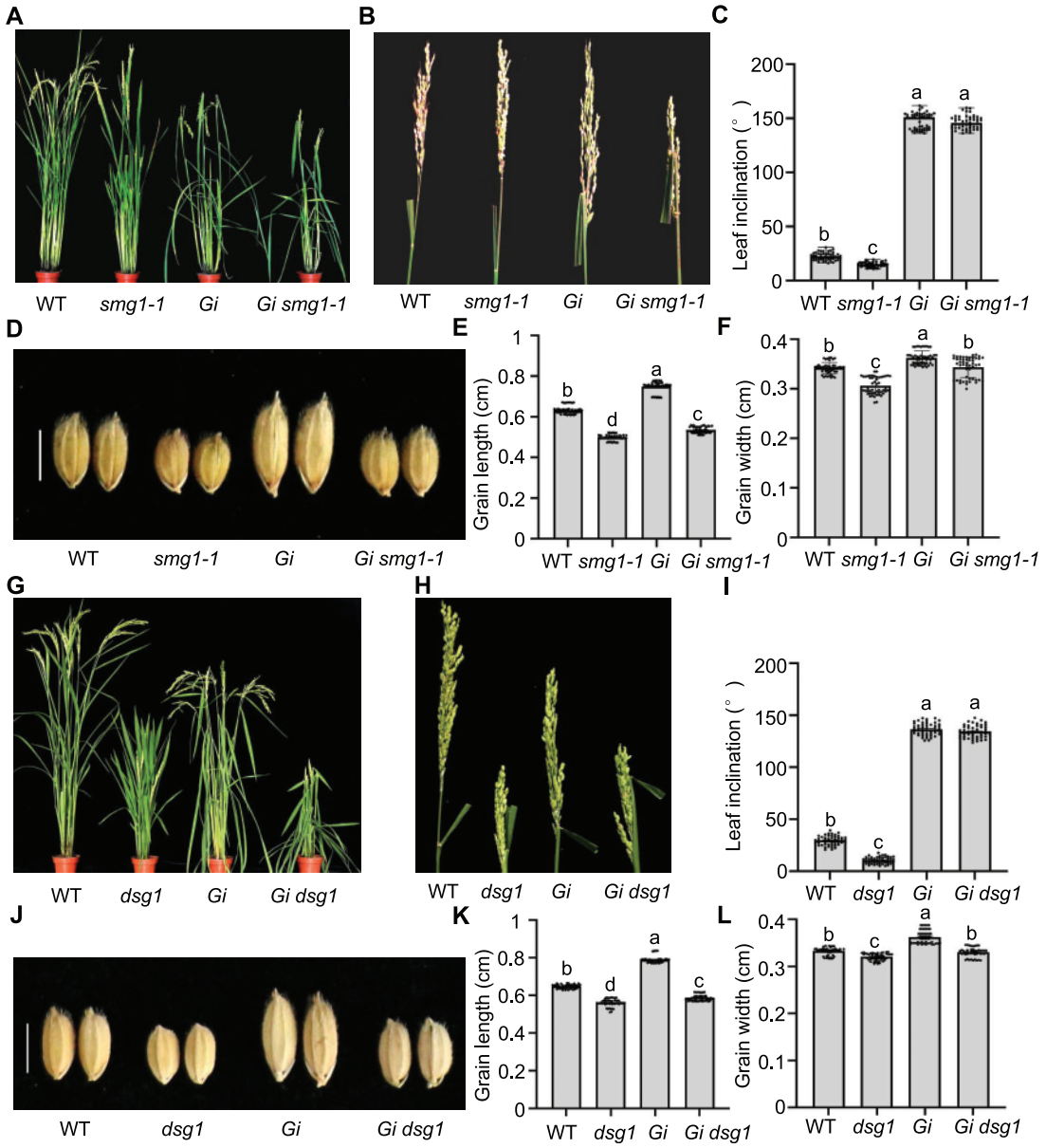

Figure 8 Genetic relationship of MAPKK4−MAPK6 and GSK2. A–C, Gross morphology (A), flag leaf angles (B), and quantification of leaf angles (C) of WT, *smg1-1*, *Gi*, and *Gi smg1-1* at heading stage. D–F, Grain morphology (D), quantification of grain length (E), and grain width (F) in WT, *smg1-1*, *Gi*, *Gi smg1-1*, respectively (scale bar = 5 mm). G–I, Gross morphology (G), flag leaf angles (H), and quantification of leaf angles (I) of WT, *dsg1*, *Gi*, and *Gi dsg1* at heading stage. J–L, Grain morphology (J), quantification of grain length (K), and grain width (L) in WT, *dsg1*, *Gi*, and *Gi dsg1*, respectively (scale bar = 5 mm). Each dot represents the result from one biological replicate, error bars indicate means ± SE ($n = 50$). Statistically significant differences are indicated by different lowercase letters ($P < 0.05$, one-way ANOVA with Tukey's significant difference test).

line are more pronounced than in the single *WRKY53OE* or *bzr1-D* lines (Figure 4, A–H; Supplemental Figure S8, C and D). Second, in transient transfection assays, *D2* transcription rate was much lower when WRKY53 and BZR1 were co-expressed relative to the simple transfection of WRKY53 or BZR1 (Figure 5F). These results suggest that WRKY53 functions synergistically with BZR1. Third, the *bzr1-1D wrky53* line is phenotypically similar to the *bzr1-D* line in terms of leaf angle, gross morphology, and the expression pattern of BR marker genes (Figure 4, I–L). Fourth, the *wrky53* mutant failed to repress *D2* transcription mediated by BZR1 when the effector was supplied at higher DNA amounts (Figure 5G). These results suggest that the loss of WRKY53 function cannot suppress BZR1 function, and that WRKY53 does not act downstream of BZR1, indicating that they may in fact function in parallel. Fifth, the W-box and BRRE-box promoter motifs were significantly enriched in the promoter regions of genes co-regulated by WRKY53 and GSK2 (Supplemental Figure S11). These results imply that WRKY53 functions in parallel with BZR1 to co-regulate the expression of their common targets. In future work, investigating the WRKY53 transcriptional regulatory network and

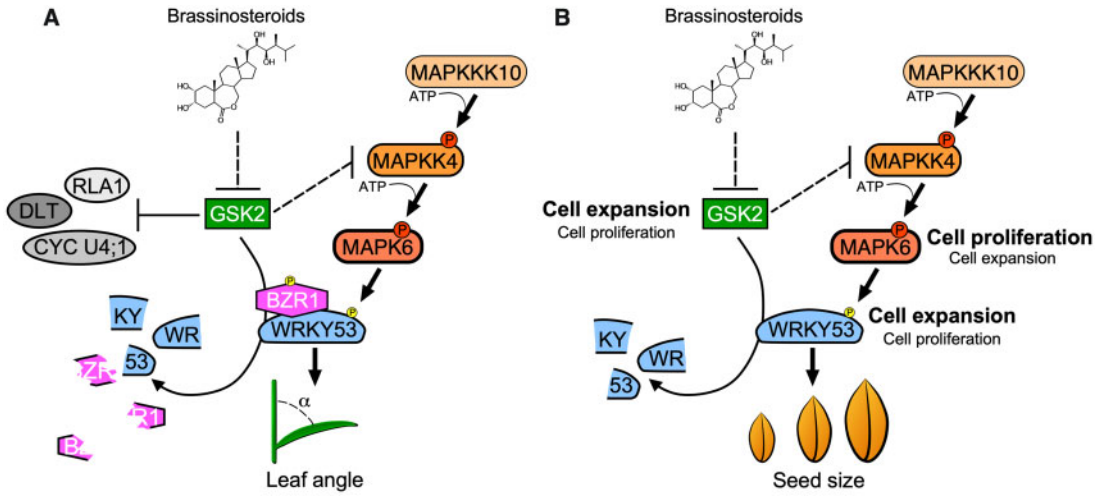

Figure 9 Proposed working model for the role of WRKY53 in BR signaling and MAPK pathway. WRKY53 is the common substrate of GSK2 and MAPK6, but functions to different degrees in BR- and MAPK-regulated seed size control and leaf angle. A, For leaf angle control, WRKY53 is major target of both BR and MAPK signaling, and WRKY53 cooperate with BZR1. B, For seed size control, GSK2 and WRKY53 mainly regulate cell expansion and minorly regulate cell proliferation, while MAPK6 predominantly regulates cell proliferation and mildly regulates cell expansion, implying that WRKY53 plays a major role in BR-regulated seed size control, and a minor role in MAPK-regulated seed size control.

identifying the subsets of specific and common WRKY53 and BZR1 targets will be a prerequisite before beginning to uncover how WRKY53 and BZR1 function together in rice BR signaling.

In addition, WRKY53 can interact with BZR1 and function in parallel and synergistically to regulate BR signaling (Figures 4 and 5; Supplemental Figures S8–S11). This situation is similar to the known relationship between Arabidopsis WRKY46/54/70 and BZR1 (Chen et al., 2017), although Arabidopsis WRKY46/54/70 are not quite equivalent to WRKY53 (Tian et al., 2017). Several GSK2 substrates have been characterized: BZR1, RLA/SMOS1, and DLT/SMOS2 were shown to co-regulate the expression of downstream genes and participate in BR signaling (Bai et al., 2007; Hirano et al., 2017; Qiao et al., 2017). It was also suggested that these diverse substrates may work together as a complex (Qiao et al., 2017). Thus, it will be interesting to investigate whether WRKY53 cooperates with RLA and DLT and physically interacts with them.

WRKY53 is a direct target of the MAPKKK10–MAPKK4–MAPK6 cascade

Previous studies from ours and other laboratories have shown that WRKY53 is phosphorylated by the MAPKK4–MAPK6 cascade and that MAPK6 promotes WRKY53 activity (Chujo et al., 2014; Hu et al., 2015; Tian et al., 2017). More important is that the phosphorylation of WRKY53 by MAPK6 is indispensable its function in control of leaf angle, seed size, and BR responses (Tian et al., 2017). Recently, several critical components of the MAPK pathway, including MAPKKK10, MKP1, and OsRac1, were reported to function in the control of seed size in rice by regulating MAPK6 activity (Guo et al., 2018; Xu et al., 2018a, 2018b; Zhang et al., 2019). However, there has been no direct genetic evidence to support the hypothesis that WRKY53 might be a direct substrate of MAPK6. In this study, we showed that a loss-of-function mutation in *WRKY53* suppressed the leaf angle and seed size phenotypes of transgenic *CAMAPK6* and *MKP1RNAi* lines, while the overexpression of *WRKY53* suppressed the *mapk6* and *mapkkk10* mutant phenotypes (Figure 6; Supplemental Figure S12). Combined with other studies showing that MAPKKK10, MAPKK4, and MAPK6 function in a common MAPK pathway (Guo et al., 2018; Xu et al., 2018b), we propose that WRKY53 is a direct substrate of this MAPK pathway (Figure 9, A and B). Notably, WRKY53 strongly regulates cell expansion and mildly regulates cell proliferation (Supplemental Figure S13A). Similar to a previous report, MAPK6 mainly regulated cell proliferation (Liu et al., 2015); however, analysis of *CAMAPK6*, *WRKY53SD*^{MAPK6}*OE*, and *WRKY53SA*^{MAPK6}*OE* indicated that MAPK6 might also slightly regulate cell expansion via modulating WRKY53 (Supplemental Figure S13, D–F). Combined with function of MAPK6 and WRKY53 in herbivore and pathogen response (Chujo et al., 2014; Hu et al., 2015), we propose that the MAPK6–WRKY53 cascade not only predominantly functions in leaf angle, insect, and pathogen response, but also, at least minorly, in seed size control (Figure 9, A and B). In the future, it will be interesting to identify targets for MAPK6 in regulation of cell proliferation.

Crosstalk between BR signaling and the MAPK pathway

Seed size and architecture are closely related to yield and quality (Wang et al., 2015; Zhao et al., 2018). A number of genes involved in the control of seed size have been characterized and classified into several pathways (Li et al., 2019). Both BR signaling and the MAPK pathway (MAPKKK10–

MAPKK4–MAPK6) positively regulate leaf angle and seed size (Zhang et al., 2014; Xu et al., 2018b; Li et al., 2019). However, it is currently unknown whether BR signaling and this MAPK pathway interconnect, as well as the identity of the crosstalk node. In this study, we propose that WRKY53 is a common phosphorylation substrate for the kinases GSK2 and MAPK6, therefore able to transduce signals from both BR signaling and the MAPK pathway (Figure 9, A and B). Notably, the function and effectiveness of WRKY53 in BR response and MAPK pathway are differential and dependent on specific organs and biological processes (Figure 9, A and B).

Moreover, we found that GSK2 can phosphorylate MAPKK4 and then decrease MAPK6 activity (Figure 7). Although the leaf angle phenotype does not support that GSK2 functions upstream of MAPK6 cascade (Figure 8; Supplemental Figure S12). Since GSK2 has multiple substrates to control diverse processes (Tong and Chu, 2018), mutation of a single MAPK signaling component is not enough to reverse all GSK2 function. Our results do not rule out the possibility that GSK2 functions upstream of MAPK in some specific processes, similar to the way BIN2 phosphorylates MAPKK4 and then represses MAPK6 activity to mediate BR-regulated stomatal development (Khan et al., 2013). In addition, since neither GSK2, MAPKK4, nor MAPK6 exhibit a clear tissue-specific expression pattern (Supplemental Figure S17), and considering that GSK2 phosphorylates multiple substrates and plays key roles in various developmental processes (Bai et al., 2007; Tong et al., 2012; Sun et al., 2015; Yang et al., 2016; Qiao et al., 2017; Xiao et al., 2017), we speculate that GSK2 may deploy different substrates to regulate diverse developmental processes in a tissue- or organ-specific manner.

Differential mechanism of WRKY53 phosphorylation by MAPK6 and GSK2

While WRKY53 is phosphorylated by both GSK2 and MAPK6, the effects of these two phosphorylation events may be distinct. WRKY53 phosphorylation by GSK2 lowered WRKY53 stability (Figures 2 and 3); conversely, bikinin treatment stabilized WRKY53 (Figure 2G). These results help explain how WRKY53 accumulates in response to BR signaling: via the negative regulation of GSK2. Our previous study showed that WRKY53 is phosphorylated by the MAPKK4–MAPK6 cascade. The overexpression of $WRKY53SD^{MAPK6}$ (a phospho-mimic of constitutive phosphorylation by MAPK6) displayed a much stronger BR-related phenotype than did the overexpression of wild-type *WRKY53*. Notably, MAPK6 increased the DNA binding affinity of WRKY53 (Tian et al., 2017). These results suggest that WRKY53 phosphorylation by MAPK6 significantly promotes WRKY53 activity, in contrast to its phosphorylation by GSK2, which results in WRKY53 destabilization. Interestingly, WRKY53 also represses the expression of its encoding gene as well as *MAPK6* (Hu et al., 2015; Tian et al., 2017), suggesting that WRKY53 fine-tunes BR signaling and the MAPK pathway.

Materials and methods

Plant materials and growth conditions

Rice cultivar LJ11, Nipponbare (NP), Kuanyejing (KYJ), and ZH11 (*Oryza sativa* ssp. *japonica*) were used as wild-type control to compare with diverse mutants or overexpression plants in relative background. *Gi* and *Go* plant (Tong et al., 2012), *BZR1* overexpression plant (*bzr1-D*) (Qiao et al., 2017), *MAPK6* mutant *dsg1* (Liu et al., 2015), *MAPKK4* mutant *smg1-1* (Duan et al., 2014), *CAMAPK6* overexpression plant, and *MAPKKK10* mutant *smg2-1* (Xu et al., 2018b), *WRKY53* overexpression plant *WRKY53OE* and *wrky53* mutant (Tian et al., 2017), and *MKP1RNAi* plant were used to develop double mutants. Plants were grown in the field (natural long-day conditions) or growth chamber (white fluorescent tubes, 200–300 μmol m^{-2} s^{-1}) at 30°C for 14 h (day) and 24°C for 10 h (night).

Generation of transgenic and double mutant plants

To generate the *WRKY53OE* and *wrky53* mutant in different backgrounds, the *WRKY53* overexpression vector (*Ubiquitin:WRKY53*) and *WRKY53* gene editing vectors were used for transformation (Tian et al., 2017). *Ubiquitin:WRKY53* was transformed into *dsg1* and *smg2-1* to generate *dsg1 WRKY53OE* and *smg2-1 WRKY53OE*, respectively. For creating *Gi wrky53* and *bzr1-D wrky53*, *WRKY53* gene-editing vectors were transformed into *Gi* and *bzr1-D*, respectively. *CAMAPK6* and *wrky53* were crossed to generate *CAMAPK6 wrky53*. To create *MKP1RNAi wrky53*, we generated *MKP1RNAi* plants and crossed them with *wrky53*. *Gi* and *WRKY53OE* were crossed to generate *Gi WRKY53OE*. *bzr1-D* and *WRKY53OE* were crossed to generate *bzr1-D WRKY53OE*. *Gi* was crossed with *smg1-1* and *dsg1* to generate *Gi smg1-1* and *Gi dsg1*, respectively. To generate *MYC-WRKY53OE*, *MYC-WRKY53(SA)OE*, and *MYC-WRKY53(SD)OE*, *WRKY53*, *WRKY53(SA)*, and *WRKY53(SD)* in *pENTRY* vector were cloned into *pGWB18* through LR recombination reaction. For all these mutants, the mutation site and expression level of corresponding genes were examined by DNA sequence, RT-qPCR, or immunoblot.

Lamina joint assay

The lamina joint assay using excised leaf segments was performed as described previously (Tian et al., 2017). Simply, uniform germinated seeds were selected and grown in the dark for 8 days at 30°C. The entire segments comprising 1 cm of the second leaf blade, the lamina joint, and 1 cm of the leaf sheath were incubated in various concentrations of 24-epiBL for 48 h in dark. The angles of lamina joint bending were measured using ImageJ software (http://rsbweb.nih.gov/ij/).

Scanning electron microscope analysis

Mature seeds were scanned with an electron microscope (JSM-IT500). The cell number in the central part of the lemma was counted in the longitudinal axis by ImageJ

software. The average longitudinal cell length was calculated by dividing the seed length by the number of cells.

Total RNA isolation and RT-qPCR analysis

Total RNA was extracted using TRIzol (Invitrogen, Carlsbad, CA, USA) and treated with DNaseI. cDNA was synthesized from 2 μg of total RNA using SuperscriptII Reverse Transcriptase (Invitrogen). Real-time PCR was performed with SYBR Green PCR master mix (Takara, Kyoto, Japan). Data were collected using Bio-Rad chromo four real-time PCR detector. All expressions were normalized against the *ubiquitin* gene (*Os01g0328400*). The primers used are listed at Supplemental Data Set S4. Three biological repeats were performed for each analysis. Values are means ± SE of three biological repeats.

BiFC assay

For BiFC assays, GSK2, BZR1, MAPKK4, WRKY53, negative control MAPKK6, and WRKY81 were fused with partial GFP; *nGFP-GSK2*, *nGFP-BZR1*, *nGFP-MAPKK4*, *nGFP-MAPKK6*, *cGFP-GSK2*, *cGFP-WRKY53*, and *cGFP-WRKY81* were generated as described in Supplemental Data Set S4. These vectors were transformed into *Agrobacterium* strain GV3101 and co-injected into young leaves of *N. benthamiana*. The fluorescence was observed by confocal microscopy (Leica, Wetzlar, Germany) after 2 days growth. At least three biological replicates with five left in a replicate were performed. For each replicate, at least three discs were randomly selected from infiltrated leaves and imaged. There are around 10 or more interactions out of 100 cells in each area screened. Discs were imaged and interactions were observed, and a represent image is shown.

LCI assays

The *cLUC-WRKY53*, *cLUC-MAPKK4*, *nLUC-GSK2*, and *nLUC-BZR1* constructs were generated as shown in Supplemental Data Set S4. Agrobacteria harboring different combinations of constructs were co-infiltrated into *N. benthamiana*, and the infiltrated leaves were analyzed for LUC activity using Chemiluminescence imaging (Tanon 5200) after 48 h infiltration.

Pull-down assay

The full-length coding region of *GSK2* in *pENTR/D-TOPO* was subcloned into the expression vector *pVP13* to generate MBP-GSK2. The coding region of *MAPKK4* was introduced into *pET28a* vector to generate HIS-MAPKK4 (Supplemental Data Set S4). These constructs were expressed in *Escherichia coli* (Strain *BL21*), and the fusion proteins were purified using corresponding affinity chromatography. MBP or MBP-GSK2 coupled MBP beads were incubated with HIS-MAPKK4 for 2 h at 4°C and then washed thoroughly, boiled in 1 × SDS–PAGE sample buffer, and analyzed by immunoblot using anti-HIS antibody (OriGene, Rockville, MD, USA; TA150088) and anti-MBP antibody (CWBIO, Boston, MA, USA; CW0288M), respectively.

Co-IP assays

For Co-IP assays, *35S:mGSK2-FLAG*, *35S:MYC-WRKY53*, and *35S:Flag-BZR1* constructs were made as described in Supplemental Data Set S4. These plasmids were transiently co-expressed in rice protoplasts in the indicated combinations. The total proteins were extracted using the lysis buffer (50 mM Tris–HCl at pH 7.5, 150 mM NaCl, 0.5 mM EDTA at pH 8.0, 10% glycerol, 0.5% Triton X-100) with freshly added phenylmethylsulfonyl fluoride (PMSF; Roche, Basel, Switzerland; 10837091001), protease inhibitor cocktail (Roche; 11873580001) and MG132 (Sigma-Aldrich, St Louis, MO, USA; M8699). Before the Co-IP assays, 20 μL Protein-A/G magbeads (GenScript, Piscataway, NJ, USA; L00277) were incubated with and without 2 μL anti-Flag (Abmart, Shanghai, China; M20008) for 2 h with gentle rotation at 4°C; subsequently, extracts of equal total proteins were added incubation for 2 h at 4°C. The beads were washed 3 times with the washing buffer (50 mM Tris–HCl at pH 7.5, 100 mM NaCl, 0.5 mM EDTA at pH 8.0, 0.1% Triton X-100). The immunoprecipitates were eluted with 1×SDS sample buffer, separated on SDS–PAGE gel, transferred to PVDF membrane (Millipore, Burlington, MA, USA; 0.45 um; IPVH00010), and detected with anti-FLAG (HRP) (GenScript; A01428S), anti-FLAG (Abmart; M20008), anti-MYC (HRP; GenScript; A00863-100), and anti-MYC (ThermoFisher, Waltham, MA, USA; 9E10), respectively. For all Co-IP assays, we used two kinds of control (with and without antibody, expressing one and two proteins) and performed at least three independent replications.

In vitro kinase assays

Constructs for expression of GST-GSK2, GST-MAPKK4^{K122M}, and MBP-WRKY53 were made as described in Supplemental Data Set S4. These fusion proteins were purified according to the manufacturer's instruction. For each kinase assay, the corresponding purified proteins were incubated with phosphorylation buffer (25 mM Tris–HCl at pH 7.4, 12 mM $MgCl_2$, 1 mM DTT, and 1 mM ATP). The reactions were incubated at 30°C for 45 min and boiled in 1 × SDS loading buffer. The phosphorylation signal was detected by Phos-tag Biotin BTL-104 (Wako, Richmond, VI, USA; 301-93531) according to the manufacturer's instruction.

For in vitro MAPK assays, purified GST-GSK2, GST-MAPKK4DD, and MBP-MAPK6 (Tian et al., 2017) were incubated with phosphorylation buffer as described above. Phosphorylation of MAPK6 was detected by immunoblot with anti-phospho-p44/42 MAPK antibody (Beyotime, Nanjing, China; AM071).

In vivo MAPK activity assay

35S:GFP-mGSK2-FLAG, *35S:FLAG-MAPKK4*, and *35S:MYC-MAPK6* constructs were co-transfected into protoplasts. Different combinations of plasmid were transiently expressed in the protoplasts by PEG-mediated transfection.

Following overnight incubation in the dark at 28°C, total proteins were isolated from the protoplasts with SDS Lysis Solution (Beyotime; P0013G) with protease inhibitor cocktail (Roche; 11206893001), 50 μM MG132, 1 mM PMSF (Phenylmethanesulfonyl fluoride), and phosphatase Inhibitor Cocktail (Sigma-Aldrich; P2850). The proteins were separated by 10% SDS–PAGE and subjected to immunoblotting with anti-MYC antibody (ThermoFisher; 9E10), anti-FLAG antibody (Abmart; M20008), and anti-Phospho-p44/42 MAPK antibody (Cell Signaling Technology, Danvers, MA, USA; #9101), respectively.

Identification of phosphorylation sites

MBP-WRKY53 and GST-GSK2 were used to perform in vitro kinase assays. The phosphorylated MBP-WRKY53 was recovered from the SDS–PAGE gel and subjected to in-solution alkylation/tryptic digestion followed by liquid chromatography/tandem mass spectrometry (LC–MS/MS) as described (Qiao et al., 2017).

RNA-seq and data analysis

For Illumina sequencing, the flag leaves of ZH11, *Gi*, and *Gi wrky53* plants were collected for RNA extraction from three biological replicates. The extraction and examination of total RNA, library preparation, and Illumina sequencing were done by Novogene Bioinformatics Technology Co., Ltd., Beijing, China using the Illumina HiSeq 2500 platform. Rice cultivar NP reference genome and gene information were downloaded from IRGSP-1.0 (http://rapdb.dna.affrc.go.jp/download/irgsp.html). The mapping quality and saturation analyses were performed using Hisat2. Differentially expressed genes were detected using DESeq2 with an absolute fold change >1.5 and FDR-adjusted $P < 0.05$. The GO analysis was carried out by protein annotation through evolutionary relationship (PANTHER) classification system (www.pantherdb.org) with FDR ≤ 0.05 to get the GO annotations based on biological process. Since BR-relevant genes are not all annotated in PANTHER protein class database, the enrichment of BR-relevant genes for the protein class was manually calculated using Fisher's exact test in R3.0.

Promoter analyses and significance calculations

We used 2,517 of 2,570 WRKY53-GSK2 co-regulated genes for promoter analysis, because 53 genes are not well annotated and have no accurate promoter sequence. Then 2000-nt-long sequence upstream of ATG as promoter regions were selected and promoter regions were extracted from rice genome sequence (https://rapdb.dna.affrc.go.jp/download/irgsp1.html Os- NP-Reference-IRGSP-1.0) by TBtools (https://github.com/CJ-Chen/TBtools). A promoter database set containing promoters for 2,517 genes was then created. To identify overrepresented promoter elements, W-box (TTGACT/C), BRRE (CGTGT/CG), and E-box (CATGTG) elements in promoter regions were identified using MEME (http://meme-suite.org/tools/fimo). One hundred surrogates for each promoter database set were created by randomly selecting genes that are not included in WRKY53 and GSK2 co-regulated genes. We modeled the null distribution for each motif by counting the number of occurrences for each motif within each of the 100 surrogate sets. The one-tailed *P*-value for each motif was estimated based on the Z-score of the difference of the actual word count of the promoter set (C_{true}) minus the mean count from the 100 surrogates (C_{rand}) relative to theSD from the 100 surrogates (SD_{rand}) (i.e. $Z = [C_{true} - C_{rand}]/SD_{rand}$). By means of this Z-score, we obtained the probability for each motif to be over-represented compared with random number of occurrences.

Protein gel blot analysis

For the secondary antibody in the protein gel blot assay, peroxidase-labeled goat anti-rabbit antibody (Abcam; ab6721) or goat anti-mouse antibody (Abcam; ab6789) was utilized. Membranes were developed with the Super signal west pico chemiluminescent substrate kit (Pierce Biotechnology, Rockford, IL, USA) and the signal was detected by chemiluminescence imaging (Tanon 5200).

WRKY53 stability assays

35S:mGSK2-FLAG and *35S:MYC-WRKY53* constructs were co-transfected into protoplasts. For bikinin treatment assay, protoplasts transformed with the destination vector were treated with 40 μM bikinin (Selleckchem.com) for 16 h. For BR treatment assay, the protoplasts transformed with the destination vector were cultured for 12 h and then treated with 24-epiBL (Sigma, Kanagawa, Japan; E1641) for 30 min.

Transient transcription dual-LUC assays

The *35S:WRKY53* and *35S:BZR1* constructs were generated and used as effector, and the promoter region (upstream of the ATG) of *D2* was cloned into *pGreenII 0800-LUC* vector and used as reporter (Supplemental Data Set S4). The resulting effector and reporter constructs were co-transformed into protoplasts. The *Renilla* (*REN*) *LUC* gene directed by *35S* promoter in the *pGreenII 0800-LUC* vector was used as an internal control. Firefly LUC and REN activities were measured with a Dual-LUC reporter assay kit (Beyotime; RG027) using a GloMax 20/20 luminometer (Promega, Madison, WI, USA). The LUC activity was normalized to REN activity and LUC/REN ratios were calculated. For each plasmid combination, at least three independent transformations were performed. Values are means ± SE of independent biological repeats.

EMSAs

MBP-WRKY53 recombinant proteins were affinity purified and used (Tian et al., 2017). About 40-bp oligonucleotide probes containing wild-type W-box (TGACC) or mutated W-box (AAAAA) motifs were synthesized and labeled with biotin using EMSA Probe Biotin Labeling Kit (Beyotime; Cat No GS008). For nonlabeled probe competition, nonlabeled probe was added to the reactions. EMSA was performed using a Chemiluminescent EMSA kit (Beyotime; Cat No

GS009). Probe sequences are shown in Supplemental Data Set S4.

Statistical analysis

One-way ANOVA with Tukey's honestly significant differences test was used to evaluate the differences across multiple samples, and statistically significant differences are indicated by different lowercase letters, $P < 0.05$. ANOVA results are listed in Supplemental Data Set S5.

Data availability

The RNA-seq data of this article have been submitted to the National Center for Biotechnology Information Gene Expression Omnibus (https://www.ncbi.nlm.nih.gov/geo/query/acc.cgi) and was assigned with the following identification accession numbers: GSE148099.

Accession numbers

Sequence data from this article can be found in the GenBank/EMBL database under the following accession numbers: WRKY53, Os05g0343400; GSK2, Os05g0207500; BZR1, Os07g0580500; MAPKK4, Os02g0787300; MAPK6, Os06g0154500; MAPKK6, Os01g0510100; WRKY81, LOC_Os12g02400.1; MKP1, Os05g0115800; D2, Os01g0197100; DWARF4, Os03g0227700; BRD1, Os03g0602300; D11, Os04g0469800; CYP93G2, Os06g0102100; CYP76M7, Os09g0528700; CYP97C2, Os10g0546600; ERD1, Os02g0526400; WRKY72, Os11g0490900; Cyc1, Os04g0178300; Ubiquitin, Os01g0328400.

Supplemental data

The following materials are available in the online version of this article.

Supplemental Figure S1. Identification of *Gi wrky53* mutant.

Supplemental Figure S2. *wrky53* reverses the enlarged leaf angle of *Gi*.

Supplemental Figure S3. Phenotypic analysis of *Gi WRKY53OE*.

Supplemental Figure S4. RNA-seq data analysis.

Supplemental Figure S5. RT-qPCR assay confirming the expression of genes oppositely regulated by GSK2 and WRKY53.

Supplemental Figure S6. Identification of WRKY53 phosphorylation Sites by GSK2 kinase using LC–MS/MS.

Supplemental Figure S7. Phenotypes of the *MYC-WRKY53(SA)OE* and *MYC-WRKY53(SD)OE*.

Supplemental Figure S8. Identification and phenotypic analysis of *bzr1-D WRKY53OE* double mutant.

Supplemental Figure S9. Identification and phenotypic analysis of *bzr1-D wrky53* double mutant.

Supplemental Figure S10. WRKY53 binds to *D2* promoter in vitro.

Supplemental Figure S11. Promoter analysis of WRKY53 and GSK2 co-regulated genes.

Supplemental Figure S12. WRKY53 genetically acts downstream of MAPK6.

Supplemental Figure S13. Epidermal cell analysis.

Supplemental Figure S14. Amino acid sequence of MAPKK4.

Supplemental Figure S15. Identification and phenotypic analysis of *Gi smg1-1* double mutant.

Supplemental Figure S16. Identification and phenotypic analysis of *Gi dsg1* double mutant.

Supplemental Figure S17. Tissue-specific expression pattern analysis of *GSK2*, *MAPKK4*, and *MAPK6*.

Supplemental Data Set S1. Analysis of differentially expressed genes in RNA-seq.

Supplemental Data Set S2. Analysis of GSK2- and WRKY53- regulated genes.

Supplemental Data Set S3. Un-cropped images of protein gel blots in this paper.

Supplemental Data Set S4. Primers used in this work.

Supplemental Data Set S5. ANOVA analysis from this work.

Acknowledgments

We thank Prof. Chengcai Chu, Prof. Yunhai Li, Prof. Xuelu Wang, Prof. Fan Chen, and Prof. Hongning Tong for providing the relative mutants and vectors. We also thank Prof. Dongping Lv, and Prof. Jiuhai Zhao for their assistance in phosphorylation assay and RNA-seq analysis, and Dr. Xiangbing Meng for rice transformation.

Funding

This study was supported by National Natural Science Foundation of China (Grant No. 31671653, 31801017, and 31871591), Youth Innovation Promotion Association CAS (Grant No. 2021229), National Natural Science Foundation of China-Heilongjiang Joint Fund (Grant No. U20A2025), Strategic Priority Research Program of Chinese Academy of Sciences (Grant No. XDA24040102), and Natural Science Foundation of Heilongjiang Province (Grant No. JQ2020C003).

*Conflict of interest statement.*The authors declare no conflicts of interest.

References

Bai MY, Zhang LY, Gampala SS, Zhu SW, Song WY, Chong K, Wang ZY (2007). Functions of OsBZR1 and 14-3-3 proteins in brassinosteroid signaling in rice. Proc Natl Acad Sci USA **104:** 13839–13844

Che R, Tong H, Shi B, Liu Y, Fang S, Liu D, Xiao Y, Hu B, Liu L, Wang H, et al. (2015). Control of grain size and rice yield by GL2-mediated brassinosteroid responses. Nat Plants **2**: 15195

Chen J, Nolan TM, Ye H, Zhang M, Tong H, Xin P, Chu J, Chu C, Li Z, Yin Y (2017) *Arabidopsis* WRKY46, WRKY54, and WRKY70 transcription factors are involved in brassinosteroid-regulated plant growth and drought responses. Plant Cell **29:** 1425–1439

Chujo T, Miyamoto K, Ogawa S, Masuda Y, Shimizu T, Kishi-Kaboshi M, Takahashi A, Nishizawa Y, Minami E, Nojiri H, et

al. (2014) Overexpression of phosphomimic mutated OsWRKY53 leads to enhanced blast resistance in rice. PLoS One **9:** e98737

Duan P, Rao Y, Zeng D, Yang Y, Xu R, Zhang B, Dong G, Qian Q, Li Y (2014) *SMALL GRAIN 1*, which encodes a mitogen-activated protein kinase kinase 4, influences grain size in rice. Plant J **77:** 547–557

Gao X, Zhang JQ, Zhang X, Zhou J, Jiang Z, Huang P, Tang Z, Bao Y, Cheng J, Tang H, et al. (2019) Rice qGL3/OsPPKL1 functions with the GSK3/SHAGGY-like kinase OsGSK3 to modulate brassinosteroid signaling. Plant Cell **31:** 1077–1093

Guo T, Chen K, Dong NQ, Shi CL, Ye WW, Gao JP, Shan JX, Lin HX (2018) GRAIN SIZE AND NUMBER1 negatively regulates the OsMKKK10-OsMKK4-OsMPK6 cascade to coordinate the trade-off between grain number per panicle and grain size in rice. Plant Cell **30:** 871–888

He JX, Gendron JM, Yang Y, Li J, Wang ZY (2002) The GSK3-like kinase BIN2 phosphorylates and destabilizes BZR1, a positive regulator of the brassinosteroid signaling pathway in Arabidopsis. Proc Natl Acad Sci USA **99:** 10185–10190

Hirano K, Yoshida H, Aya K, Kawamura M, Hayashi M, Hobo T, Sato-Izawa K, Kitano H, Ueguchi-Tanaka M, Matsuoka M (2017) SMALL ORGAN SIZE 1 and SMALL ORGAN SIZE 2/DWARF AND LOW-TILLERING form a complex to integrate auxin and brassinosteroid signaling in rice. Mol Plant **10:** 590–604

Hu L, Ye M, Li R, Zhang T, Zhou G, Wang Q, Lu J, Lou Y (2015) The rice transcription factor WRKY53 suppresses herbivore-induced defenses by acting as a negative feedback modulator of mitogen-activated protein kinase activity. Plant Physiol **169:** 2907–2921

Hu X, Qian Q, Xu T, Zhang Y, Dong G, Gao T, Xie Q, Xue Y (2013) The U-box E3 ubiquitin ligase TUD1 functions with a heterotrimeric G alpha subunit to regulate brassinosteroid-mediated growth in rice. PLoS Genet **9:** e1003391

Hu Z, Lu SJ, Wang MJ, He H, Sun L, Wang H, Liu XH, Jiang L, Sun JL, Xin X, et al. (2018) A Novel QTL qTGW3 encodes the GSK3/SHAGGY-like kinase OsGSK5/OsSK41 that interacts with OsARF4 to negatively regulate grain size and weight in rice. Mol Plant **11:** 736–749

Jang S, An G, Li HY (2017) Rice leaf angle and grain size are affected by the OsBUL1 transcriptional activator complex. Plant Physiol **173:** 688–702

Khan M, Rozhon W, Bigeard J, Pflieger D, Husar S, Pitzschke A, Teige M, Jonak C, Hirt H, Poppenberger B (2013) Brassinosteroid-regulated GSK3/Shaggy-like kinases phosphorylate mitogen-activated protein (MAP) kinase kinases, which control stomata development in *Arabidopsis thaliana*. J Biol Chem **288:** 7519–7527

Kim TW, Wang ZY (2010) Brassinosteroid signal transduction from receptor kinases to transcription factors. Ann Rev Plant Biol **61:** 681–704

Kim TW, Guan S, Burlingame AL, Wang ZY (2011) The CDG1 kinase mediates brassinosteroid signal transduction from BRI1 receptor kinase to BSU1 phosphatase and GSK3-like kinase BIN2. Mol Cell **43:** 561–571

Kim TW, Michniewicz M, Bergmann DC, Wang ZY (2012) Brassinosteroid regulates stomatal development by GSK3-mediated inhibition of a MAPK pathway. Nature **482**: 419–422

Kim TW, Guan S, Sun Y, Deng Z, Tang W, Shang JX, Burlingame AL, Wang ZY (2009) Brassinosteroid signal transduction from cell-surface receptor kinases to nuclear transcription factors. Nat Cell Biol **11:** 1254–1260

Koh S, Lee SC, Kim MK, Koh JH, Lee S, An G, Choe S, Kim SR (2007) T-DNA tagged knockout mutation of rice OsGSK1, an orthologue of Arabidopsis BIN2, with enhanced tolerance to various abiotic stresses. Plant Mol Biol **65:** 453–466

Li D, Wang L, Wang M, Xu YY, Luo W, Liu YJ, Xu ZH, Li J, Chong K (2009) Engineering OsBAK1 gene as a molecular tool to improve rice architecture for high yield. Plant Biotechnol J **7:** 791–806

Li J, Chory J (1997) A putative leucine-rich repeat receptor kinase involved in brassinosteroid signal transduction. Cell **90:** 929–938

Li J, Wen J, Lease KA, Doke JT, Tax FE, Walker JC (2002) BAK1, an *Arabidopsis* LRR receptor-like protein kinase, interacts with BRI1 and modulates brassinosteroid signaling. Cell **110:** 213–222

Li N, Xu R, Li Y (2019) Molecular networks of seed size control in plants. Ann Rev Plant Biol **70:** 435–463

Liu S, Hua L, Dong S, Chen H, Zhu X, Jiang J, Zhang F, Li Y, Fang X, Chen F (2015) OsMAPK6, a mitogen-activated protein kinase, influences rice grain size and biomass production. Plant J **84:** 672–681

Morinaka Y, Sakamoto T, Inukai Y, Agetsuma M, Kitano H, Ashikari M, Matsuoka M (2006) Morphological alteration caused by brassinosteroid insensitivity increases the biomass and grain production of rice. Plant Physiol **141:** 924–931

Qiao S, Sun S, Wang L, Wu Z, Li C, Li X, Wang T, Leng L, Tian W, Lu T, et al. (2017) The RLA1/SMOS1 transcription factor functions with OsBZR1 to regulate brassinosteroid signaling and rice architecture. Plant Cell **29:** 292–309

Sakamoto T, Morinaka Y, Ohnishi T, Sunohara H, Fujioka S, Ueguchi-Tanaka M, Mizutani M, Sakata K, Takatsuto S, Yoshida S, et al. (2006) Erect leaves caused by brassinosteroid deficiency increase biomass production and grain yield in rice. Nat Biotechnol **24:** 105–109

Sun S, Chen D, Li X, Qiao S, Shi C, Li C, Shen H, Wang X (2015) Brassinosteroid signaling regulates leaf erectness in *Oryza sativa* via the control of a specific U-type cyclin and cell proliferation. Dev Cell **34:** 220–228

Sun Y, Han Z, Tang J, Hu Z, Chai C, Zhou B, Chai J (2013) Structure reveals that BAK1 as a co-receptor recognizes the BRI1-bound brassinolide. Cell Res **23:** 1326–1329

Sun Y, Fan XY, Cao DM, Tang W, He K, Zhu JY, He JX, Bai MY, Zhu S, Oh E, et al. (2010) Integration of brassinosteroid signal transduction with the transcription network for plant growth regulation in *Arabidopsis*. Dev Cell **19:** 765–777

Tanaka A, Nakagawa H, Tomita C, Shimatani Z, Ohtake M, Nomura T, Jiang CJ, Dubouzet JG, Kikuchi S, Sekimoto H, et al. (2009) BRASSINOSTEROID UPREGULATED1, encoding a helix-loop-helix protein, is a novel gene involved in brassinosteroid signaling and controls bending of the lamina joint in rice. Plant Physiol **151:** 669–680

Tang W, Kim TW, Oses-Prieto JA, Sun Y, Deng Z, Zhu S, Wang R, Burlingame AL, Wang ZY (2008) BSKs mediate signal transduction from the receptor kinase BRI1 in *Arabidopsis*. Science **321:** 557–560

Tian X, Li X, Zhou W, Ren Y, Wang Z, Liu Z, Tang J, Tong H, Fang J, Bu Q (2017) Transcription factor OsWRKY53 positively regulates brassinosteroid signaling and plant architecture. Plant Physiol **175:** 1337–1349

Tong H, Liu L, Jin Y, Du L, Yin Y, Qian Q, Zhu L, Chu C (2012) DWARF AND LOW-TILLERING acts as a direct downstream target of a GSK3/SHAGGY-like kinase to mediate brassinosteroid responses in rice. Plant Cell **24:** 2562–2577

Tong H, Jin Y, Liu W, Li F, Fang J, Yin Y, Qian Q, Zhu L, Chu C (2009) DWARF AND LOW-TILLERING, a new member of the GRAS family, plays positive roles in brassinosteroid signaling in rice. Plant J **58:** 803–816

Tong H, Chu C (2018) Functional specificities of brassinosteroid and potential utilization for crop improvement. Trends Plant Sci **23:** 1016–1028

Wang S, Li S, Liu Q, Wu K, Zhang J, Wang S, Wang Y, Chen X, Zhang Y, Gao C, et al. (2015) The OsSPL16-GW7 regulatory module determines grain shape and simultaneously improves rice yield and grain quality. Nat Genet **47:** 949–954

Wang ZY, Nakano T, Gendron J, He J, Chen M, Vafeados D, Yang Y, Fujioka S, Yoshida S, Asami T, et al. (2002) Nuclear-localized BZR1 mediates brassinosteroid-induced growth and feedback suppression of brassinosteroid biosynthesis. Dev Cell **2:** 505–513

Xiao Y, Liu D, Zhang G, Tong H, Chu C (2017) Brassinosteroids regulate OFP1, a DLT interacting protein, to modulate plant architecture and grain morphology in rice. Front Plant Sci **8:** 1698

Xu R, Yu H, Wang J, Duan P, Zhang B, Li J, Li Y, Xu J, Lyu J, Li N, et al. (2018a) A mitogen-activated protein kinase phosphatase influences grain size and weight in rice. Plant J **95:** 937–946

Xu R, Duan P, Yu H, Zhou Z, Zhang B, Wang R, Li J, Zhang G, Zhuang S, Lyu J, et al. (2018b) Control of grain size and weight by the OsMKKK10-OsMKK4-OsMAPK6 signaling pathway in rice. Mol Plant **11:** 860–873

Yamamuro C, Ihara Y, Wu X, Noguchi T, Fujioka S, Takatsuto S, Ashikari M, Kitano H, Matsuoka M (2000) Loss of function of a rice *brassinosteroid insensitive1* homolog prevents internode elongation and bending of the lamina joint. Plant Cell **12:** 1591–1606

Yang C, Shen W, He Y, Tian Z, Li J (2016) OVATE family protein 8 positively mediates brassinosteroid signaling through interacting with the GSK3-like kinase in rice. PLoS Genet **12:** e1006118

Yang CJ, Zhang C, Lu YN, Jin JQ, Wang XL (2011) The mechanisms of brassinosteroids' action: from signal transduction to plant development. Mol Plant **4:** 588–600

Yin Y, Vafeados D, Tao Y, Yoshida S, Asami T, Chory J (2005) A new class of transcription factors mediates brassinosteroid-regulated gene expression in *Arabidopsis*. Cell **120:** 249–259

Yoo SJ, Kim SH, Kim MJ, Ryu CM, Kim YC, Cho BH, Yang KY (2014) Involvement of the OsMKK4-OsMPK1 cascade and its downstream transcription factor OsWRKY53 in the wounding response in rice. Plant Pathol J **30:** 168–177

Yu X, Li L, Zola J, Aluru M, Ye H, Foudree A, Guo H, Anderson S, Aluru S, Liu P, et al. (2011) A brassinosteroid transcriptional network revealed by genome-wide identification of BESI target genes in *Arabidopsis thaliana*. Plant J **65:** 634–646

Zhang B, Wang X, Zhao Z, Wang R, Huang X, Zhu Y, Yuan L, Wang Y, Xu X, Burlingame AL, et al. (2016) OsBRI1 activates BR signaling by preventing binding between the TPR and kinase domains of OsBSK3 via phosphorylation. Plant Physiol **170:** 1149–1161

Zhang C, Bai MY, Chong K (2014) Brassinosteroid-mediated regulation of agronomic traits in rice. Plant Cell Rep **33:** 683–696

Zhang C, Xu Y, Guo S, Zhu J, Huan Q, Liu H, Wang L, Luo G, Wang X, Chong K (2012) Dynamics of brassinosteroid response modulated by negative regulator LIC in rice. PLoS Genet **8:** e1002686

Zhang LY, Bai MY, Wu J, Zhu JY, Wang H, Zhang Z, Wang W, Sun Y, Zhao J, Sun X, et al. (2009) Antagonistic HLH/bHLH transcription factors mediate brassinosteroid regulation of cell elongation and plant development in rice and *Arabidopsis*. Plant Cell **21:** 3767–3780

Zhang M, Su J, Zhang Y, Xu J, Zhang S (2018) Conveying endogenous and exogenous signals: MAPK cascades in plant growth and defense. Curr Opin Plant Biol **45:** 1–10

Zhang Y, Xiong Y, Liu R, Xue HW, Yang Z (2019) The Rho-family GTPase OsRac1 controls rice grain size and yield by regulating cell division. Proc Natl Acad Sci USA **116:** 16121–16126

Zhao DS, Li QF, Zhang CQ, Zhang C, Yang QQ, Pan LX, Ren XY, Lu J, Gu MH, et al. (2018) GS9 acts as a transcriptional activator to regulate rice grain shape and appearance quality. Nat Commun **9:** 1240